Facile Access to Redox-Active C_2-Bridged Complexes with Half-Sandwich Manganese End Groups

Sohrab Kheradmandan, Koushik Venkatesan, Olivier Blacque, Helmut W. Schmalle, and Heinz Berke*[a]

Abstract: The dinuclear mixed-valent complex $[(MeC_5H_4)(dmpe)MnC_2Mn(dmpe)(C_5H_4Me)]^+[(\eta^2\text{-}MeC_5H_4)_3Mn]^-$ $[\mathbf{1}]^+[\mathbf{2}]^-$ (dmpe = 1,2-bis(dimethylphosphanyl)ethane) was prepared by the reaction of $[Mn(MeC_5H_4)_2]$ with dmpe and $Me_3SnC{\equiv}CSnMe_3$. The reactions of $[\mathbf{1}]^+[\mathbf{2}]^-$ with $K[PF_6]$ and $Na[BPh_4]$ yielded the corresponding anion metathesis products $[(MeC_5H_4)(dmpe)MnC_2Mn(dmpe)(C_5H_4Me)][PF_6]$ ($[\mathbf{1}][PF_6]$) and $[(MeC_5H_4)(dmpe)MnC_2Mn(dmpe)(C_5H_4Me)][BPh_4]$ ($[\mathbf{1}][BPh_4]$). These mixed-valent species can be reduced to the neutral form by reaction with Na/Hg. The obtained complex $[(MeC_5H_4)(dmpe)MnC_2Mn(dmpe)(C_5H_4Me)]$ (**1**) displays a triplet/singlet spin equilibrium in solution and in the solid state, which was additionally studied by DFT calculations. The diamagnetic dicationic species $[(MeC_5H_4)(dmpe)MnC_2Mn(dmpe)(C_5H_4Me)][PF_6]_2$ ($[\mathbf{1}][PF_6]_2$) was obtained by oxidizing the mixed-valent complex $[\mathbf{1}][PF_6]$ with one equivalent of $[Fe(C_5H_5)_2][PF_6]$. Both redox processes are fully reversible. The dinuclear compounds were characterized by NMR, IR, UV-visible, and Raman spectroscopy, cyclic voltammetry, and magnetic susceptibility measurements. X-ray diffraction studies were performed on $[\mathbf{1}][\mathbf{2}]$, $[\mathbf{1}][PF_6]$, $[\mathbf{1}][BPh_4]$, and $[\mathbf{1}][PF_6]_2$.

Keywords: alkyne ligands · density functional calculations · half-sandwich complexes · manganese · mixed-valent compounds

Introduction

The field of electronics using single-molecule components has recently received much attention as a possible new path for the continued miniaturization of electronics. Molecular wires are conceptually the simplest components and basic motifs of single electron devices.[1–5] Organometallic complexes consisting of a cumulenic spacer and transition-metal end groups were anticipated to appropriately serve the fundamental requirements for the wire function.[1,4,5] Related polymers or oligomers consisting of dinuclear transition-metal units spaced by $-(C{\equiv}C)_x-$ bridges were first reported by Hagihara et al. in the late 1970 s.[7,8] Even though this earlier work has been joined by extensive preparative explorations, there is still lack of knowledge on appropriate $-(L_mM{-}C_x{-}ML_m)_n-$ species and even on their $L_mM{-}C_x{-}ML_m$ monomers. In redox wires[9–38] this electronic communication between the remote ends is related to the capability to undergo facile redox changes in conjunction with a strongly bound and electronically delocalized spacer.[6] Quite a few cases[10–15,25,32,39–78] have been studied, but there is still demand for further thorough explorations.

Redox-active metal centers combined with C_2 bridges are expected to exhibit strong through-bridge interactions. However, such species have rarely been reported.[79–93] We therefore initiated a search for C_2-bridged species with prominent redox and electron delocalization properties based on low-energy work functions. These requirements were anticipated to be well satisfied by half-sandwich molecular end groups with manganese centers bearing electron-donating phosphane and cyclopentadienyl ligands. By analogy we were able to access related redox-active dinuclear complexes of the type $[\{Mn(dmpe)_2(X)\}_2(\mu\text{-}C_4)]^n$ (X = I, C≡CH, C≡C−C≡CSiMe$_3$ and $n = 0$–$+2$),[13,67,84] but the C_2-bridged complex with, for instance, X = I could not be isolated.

Nevertheless, we then attempted the preparation of half-sandwich complexes of the type $[(MeC_5H_4)(dmpe)Mn{-}C{\equiv}C{-}Mn(dmpe)(MeC_5H_4)]^{n+}$ ($n = 0$, 1, 2) starting from the substituted manganocene $[(MeC_5H_4)_2Mn]$,[85,86] dmpe, and $Me_3SnC{\equiv}CSnMe_3$. The synthetic potential of manganocenes, in particular with regard to Cp or MeC_5H_4 replacement, has

[a] Dr. S. Kheradmandan, Dr. K. Venkatesan, Dr. O. Blacque, Dr. H. W. Schmalle, Prof. H. Berke
Anorganisch-Chemisches Institut der Universität Zürich
Winterthurerstrasse 190, 8057 Zürich, Switzerland
Fax: (+41) 163-56802
E-mail: hberke@aci.unizh.ch

Supporting information for this article is available on the WWW under http://www.chemeurj.org/ or from the author.

DOI: 10.1002/chem.200400143

not been exploited appropriately, except for an earlier work by us.[87]

Results and Discussion

Synthesis of the salt $[(MeC_5H_4)(dmpe)MnC_2Mn(dmpe)(C_5H_4Me)]^+[(\eta^2\text{-}MeC_5H_4)_3Mn]^-$ ($[1]^+[2]^-$): Treatment of $[(MeC_5H_4)_2Mn]$ with dmpe affords the pale yellow adduct $[(\eta^2\text{-}MeC_5H_4)(\eta^5\text{-}MeC_5H_4)Mn(dmpe)]$.[88] The compound was crystallized from diethyl ether/pentane at −30 °C. The X-ray crystal structure of this d^5 high-spin complex was determined (Figure 1). Remarkably, one of the methylcyclopentadienyl rings is coordinated to the metal center in an η^2 fashion, rather than in the η^5 mode suggested by Wilkinson et al.[88] This is also in contrast to the structures of related complexes $[(\eta^5\text{-}C_5H_5)_2Mn(dmpe)]$ (dmpe = 1,2-bis(dimethylphosphino)ethane),[85,86] $[(\eta^5,\eta^1\text{-}C_5H_5)_2Mn(tmeda)]$ and $[(\eta^1,\eta^1\text{-}MeC_5H_4)_2Mn(tmeda)]$ (tmeda = *N*,*N*,*N*′,*N*′-tetramethyl 1,2-ethanediamine),[88,89] in which other hapticities of the Cp rings occur. It was not possible to provide evidence for the hapticity of the cyclopentadienyl rings in solution, since the ^1H NMR spectrum shows strong line broadening due to the paramagnetism of these species. The low hapticities of the Cp rings, which we assumed to prevail also in solution, may be supportive of the facile ring displacements exploited in the following reactions.

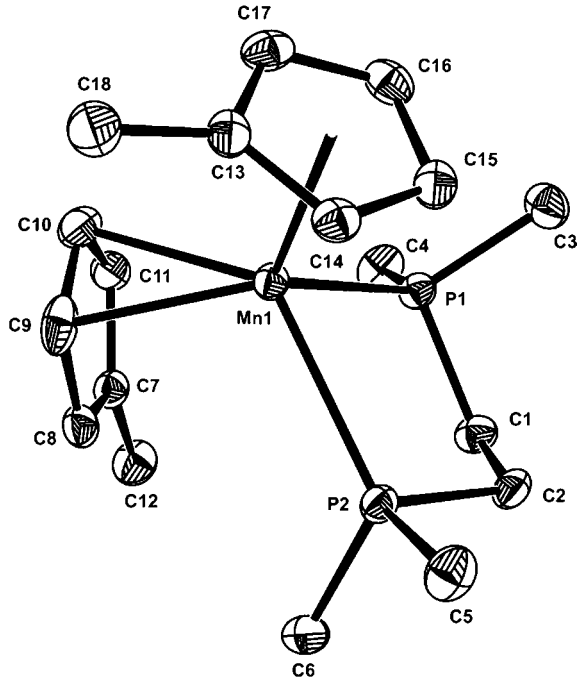

Figure 1. Molecular structure of $[(\eta^2\text{-}MeC_5H_4)(\eta^5\text{-}MeC_5H_4)Mn(dmpe)]$ (30 % probability displacement ellipsoids). Selected bond lengths [Å] and angles [°]: Mn1−C9 2.374(2), Mn1−C10 2.409(2), Mn1−P1 2.6646(6), Mn1−P2 2.7153(6); C9-Mn1-C10 34.19(8), C9-Mn1-P1 128.92(6), C10-Mn1-P1 108.78(7), C9-Mn1-P2 103.96(7), C10-Mn1-P2 131.54(6). Hydrogen atoms are omitted for clarity.

The reaction of $Me_3SnC{\equiv}CSnMe_3$ with two equivalents of $[(\eta^2\text{-}MeC_5H_4)(\eta^5\text{-}MeC_5H_4)Mn(dmpe)]$ in THF at room temperature did not yield the expected $[(MeC_5H_4)(dmpe)MnC_2Mn(dmpe)(C_5H_4Me)]$ (**1**); instead, its oxidized mixed-valent form $[\mathbf{1}]^+$ was obtained in combination with the trigonally coordinated high-spin anion $[(\eta^2\text{-}MeC_5H_4)_3Mn]^-$ (**2**), which was described earlier by us.[90] The brown paramagnetic product $[\mathbf{1}]^+[\mathbf{2}]^-$ was isolated in a 67 % theoretical yield based on $[(MeC_5H_4)_2Mn]$ and the given stoichiometry of Scheme 1. The formation of this peculiar pair of complexes can be rationalized on the basis of strongly reducing properties of neutral **1**, which may indeed form first. Subsequent electron transfer occurs from **1** to an intermediate Mn^{II} complex cation $[(MeC_5H_4)(dmpe)Mn(\eta^1\text{-}dmpe)]^+$ to form the very stable complex $[\{(MeC_5H_4)(dmpe)Mn\}_2(\mu\text{-}dmpe)]$ (**3**) and dmpe. Formation of the intermediate cation can be envisaged by ligand disproportionation starting from

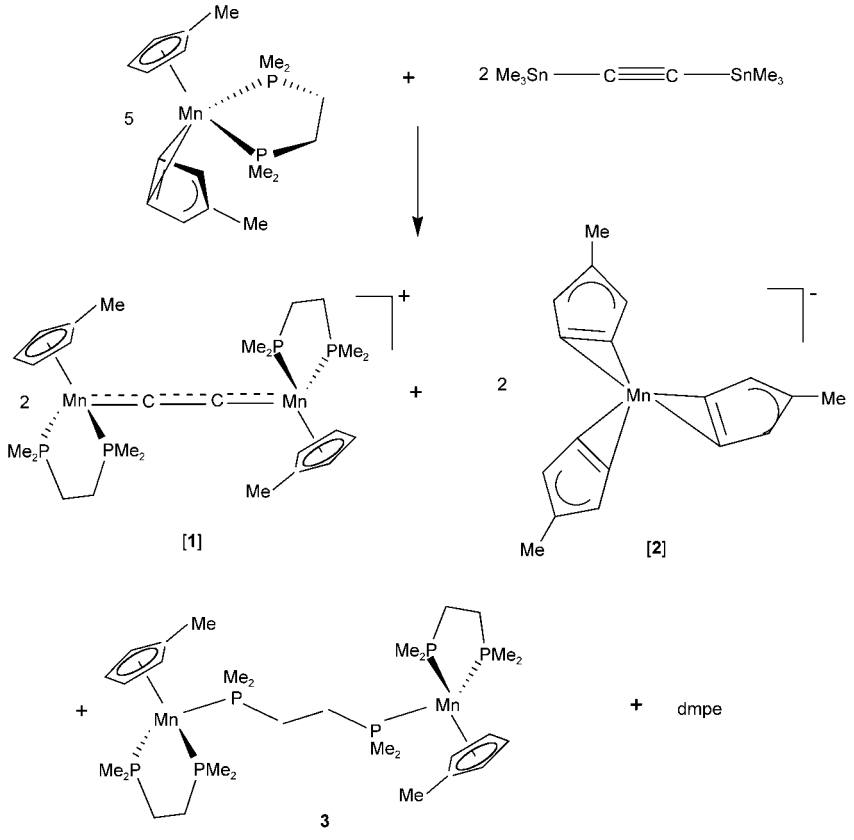

Scheme 1.

$[(\eta^2\text{-}MeC_5H_4)(\eta^5\text{-}MeC_5H_4)Mn(dmpe)]$ [Eq. (1)], which also makes **2** available.

$$2\,[(MeC_5H_4)_2Mn(dmpe)] \rightleftharpoons [(MeC_5H_4)(dmpe)Mn(\eta^1\text{-}dmpe)]^+ + [(\eta^2\text{-}MeC_5H_4)_3Mn]^- \quad (1)$$

In the ^{1}H NMR spectrum of **3** the protons of the dmpe ligand were observed at 1.1–1.7 ppm. The resonances for the methylcyclopentadienyl ring appear as singlets at 3.6 and 3.8 ppm, and the methyl protons as a singlet at 2.2 ppm. The ^{31}P NMR spectrum exhibits two broad resonances at 56.0 and 87.9 ppm. Compound **3** was crystallized from diethyl ether at −30 °C and was characterized by X-ray diffraction (Figure 2).

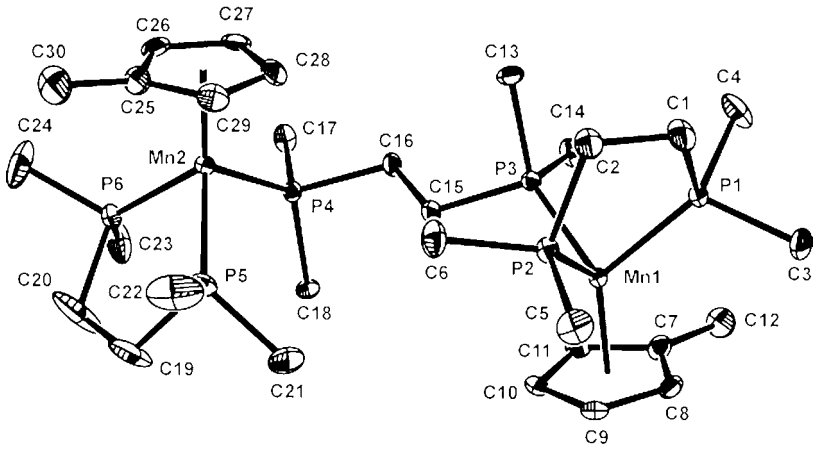

Figure 2. Molecular structure of **3** (30 % probability displacement ellipsoids). Selected bond lengths [Å] and angles [°]: Mn1−MeCp1(Cg) 2.132(3), Mn2−MeCp2(Cg) 2.132(3), Mn1−P1 2.1814(8), Mn1−P2 2.1788(8), Mn1−P3 2.2041(7), Mn2−P4 2.2090(8), Mn2−P5 2.2055(8), Mn2−P6 2.1948(8); P1-Mn1-P2 83.89(3), P2-Mn1-P3 95.83(3), P5-Mn2-P6 84.20(3), P5-Mn2-P4 99.03(3), P6-Mn2-P4 95.30(3), Mn1-P3-C15 114.20(9). Hydrogen atoms are omitted for clarity.

It was found earlier that the trigonal-planar tris(η^2-methylcyclopentadienyl)manganate anion **2** is stable only in the presence of large cations.[90] Therefore its stability in the salt [**1**][**2**] is assumed to be supported by the presence of the bulky and relatively inert counterion $[\mathbf{1}]^+$. The overall reaction forming the complex [**1**][**2**] is thus a complicated multistep process involving electron and ligand exchanges. The ^{1}H NMR spectrum of [**1**][**2**] shows broad signals for the dmpe ligand at −8.2 ppm and for the methylcyclopentadienyl protons at −7.20 and 1.1 ppm; this is expected for a mixture of paramagnetic d^5/d^4 low-spin complexes with chemical shifts in the upfield region. In accord with related investigations of Köhler et al.,[91,92a] the proton signals of the cationic part of [**1**][**2**] show a linear dependence of the chemical shifts on $1/T$, which stresses their Curie–Weiss behavior. Deep red plates of [**1**][**2**] were obtained by slow diffusion of diethyl ether into a saturated solution of the complex in THF. The structure of [**1**][**2**] was determined by X-ray diffraction (Figure 3).

Anion metathesis of $[\mathbf{1}]^+[\mathbf{2}]$ with $[PF_6]^-$ and $[BPh_4]^-$: Treatment of the reaction mixture of [**1**][**2**] with an excess of $K[PF_6]$ or $Na[BPh_4]$, respectively, gave the desired salts $[\mathbf{1}]^+A^-$ ($A = PF_6^-$, BPh_4^-; Scheme 2); these have good solubility in dichloromethane, while [**1**][**2**] is soluble in THF. The ^{1}H NMR spectra of [**1**][PF_6] and [**1**][BPh_4] show single resonances for the methyl group of the methylcyclopentadienyl unit at 0.3 ppm and broad superimposed high-field resonances for the dmpe and ring protons at −7.9 ppm. Both complexes were additionally characterized by single-crystal X-ray diffraction, which showed that the ion $[\mathbf{1}]^+$ has a stable structure, grossly independent of influences of the counterions. Deep red single crystals of $[\mathbf{1}]^+[BPh_4]$ suitable for X-ray studies (Figure 4) were obtained from CH_2Cl_2/THF (1/1) at −40 °C.

Redox chemistry of [1][PF_6] leading to 1 and [1][PF_6]$_2$: The mixed-valent species [**1**][PF_6] requires a strong reducing agent for its transformation into the neutral complex **1**. Thus, reduction of [**1**][PF_6] was carried out with Na/Hg in THF at room temperature for 5 h and led to the dark red neutral complex **1** (Scheme 2), which is soluble in pentane. Compound **1** is very sensitive towards oxygen and moisture and decomposes in solution within 24 h. Concentration of a solution of **1** and crystallization at −40 °C

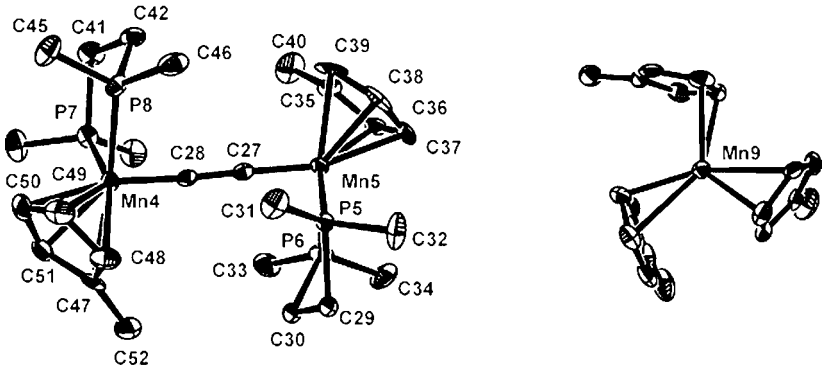

Figure 3. Molecular structure of [**1**][**2**] (30 % probability displacement ellipsoids). Selected bond lengths [Å] and angles [°]: Mn4−C28 1.790(7), C27−C28 1.312(8), Mn4−P7 2.232(2), Mn4−P8 2.217(2); C27-C28-Mn4 173.8(5), C28-Mn4-P8 86.88(18), C28-Mn4-P7 94.8(2). Seven independent molecules are found in the unit cell, of which only two are displayed for clarity. Hydrogen atoms are omitted for clarity.

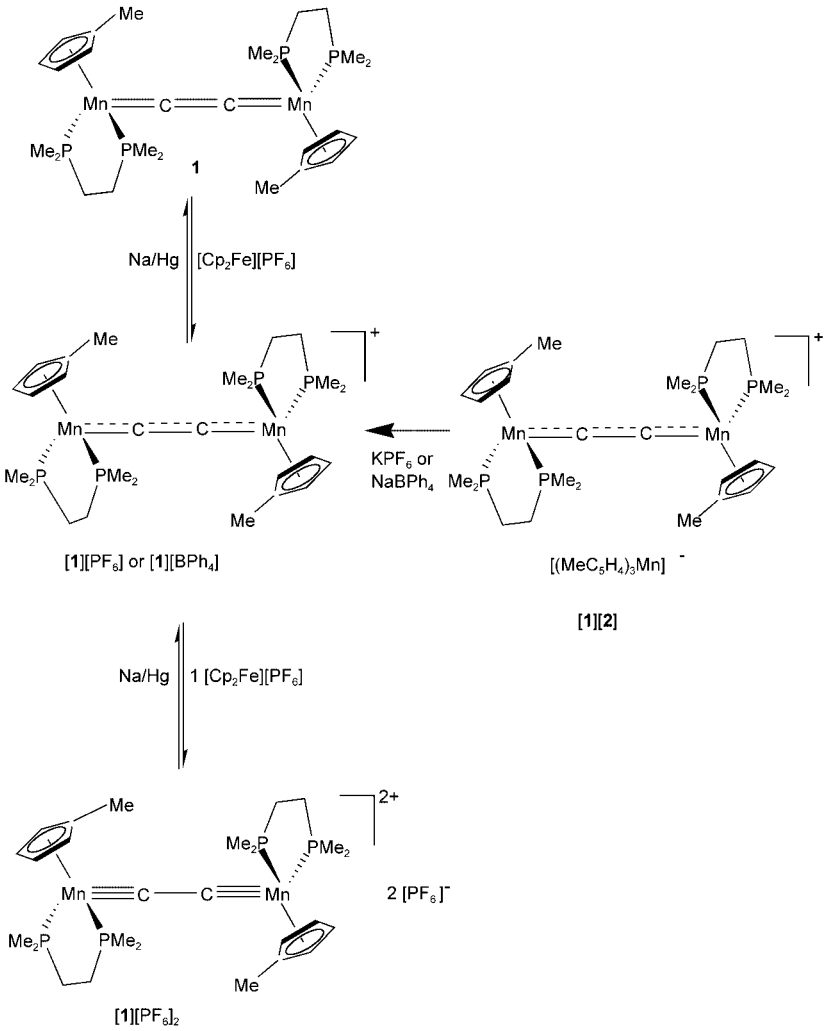

Scheme 2.

gave deep red crystals, for which an X-ray diffraction study was performed (Figure 5).

The ^{1}H NMR spectrum of **1** revealed an unusual paramagnetic behavior from room temperature down to −90 °C. At room temperature the ^{1}H NMR resonances for the methylcyclopentadienyl ring protons were observed as two sharp singlets at 4.95 and 6.67 ppm and those of the methyl protons at 2.47 ppm; both groups of resonances appeared in a chemical shift range quite consistent with that of diamagnetic compounds. However, the proton resonances for the dmpe ligand were observed at room temperature in a paramagnetically shifted range of −0.09 – 1.54 ppm. The high-field ^{31}P NMR resonance of **1** at around −21.6 ppm[84] also indicates paramagnetic influence. Variable-temperature ^{1}H NMR studies revealed that the chemical shifts of the methylcyclopentadienyl ligand were only weakly dependent on temperature, whereas the signals of the phosphorus donors exhibit a very strong temperature dependence. Variable-temperature ^{31}P NMR experiments in the range from −90 to +50 °C showed a steady shift of the signal to lower field, which finally leveled off at −90 °C.

This can be explained by assuming an equilibrium between a singlet ground state and a triplet state of **1**, with the latter at somewhat higher energy (several kcal mol^{-1}, see DFT calculations below). If thermal equilibration according to Equation (2) is fast on the NMR timescale, this leads to averaging of the signals of both species.

In the high-temperature regime of Figure 6 the triplet molecule thus prevails and causes Curie–Weiss behavior of the curve in the initial part of the $1/T$ plot, while at low temperature the singlet molecule is dominant and leads to an approximately constant ^{31}P NMR chemical shift. Note that the magnetic susceptibility measurements in the solid state (vide infra) support paramagnetic behavior of **1** due to two electrons at room temperature, but also a spin equilibrium with the singlet state, as the ground state and the triplet state in close energetic vicinity. Furthermore, the singlet state appears energetically more preferred in solution than in the solid state, owing to significant extra stabilization from a specific interaction with the solvent. To provide support for this view of equilibrating spin states in both solution and the solid state, DFT calculations were carried out on a model system (see below).

[**1**][PF_6] could be oxidized with one equivalent of [Cp_2Fe][PF_6] in CH_2Cl_2 over 24 h to [**1**][PF_6]$_2$ in quantitative yield. Complex [**1**][PF_6]$_2$ shows diamagnetic behavior. The ^{1}H NMR of [**1**][PF_6]$_2$ reveals a broad resonance for the protons of the methylcyclopentadienyl ring at 6.2 ppm, and the signal for the methyl protons appears at 2.1 ppm. The ^{31}P NMR spectrum exhibits a broad resonance at 79.3 ppm for the dmpe ligand and a septet for the [PF_6]$^-$ ion at 144.8 ppm. The deep red-brown crystals of [**1**][PF_6]$_2$ are only soluble in polar solvents like CH_3CN and CH_3NO_2. They are stable in air, which contrasts with the behavior of the complexes [**1**][PF_6] and **1**. Single crystals of [**1**][PF_6]$_2$ were obtained from CH_3CN/CH_2Cl_2/THF (2/1/1) at −40 °C (Figure 7).

DFT calculations: DFT calculations on the neutral model complex [(MeC_5H_4)(dHpe)MnC_2Mn(dHpe)(C_5H_4Me)] (**1-H**) in the gas phase revealed a paramagnetic ground state, with a singlet state at somewhat higher energy. The energy difference between the most stable conformations of the two spin states of **1-H** is only 4.5 kcal mol^{-1}. This quite small

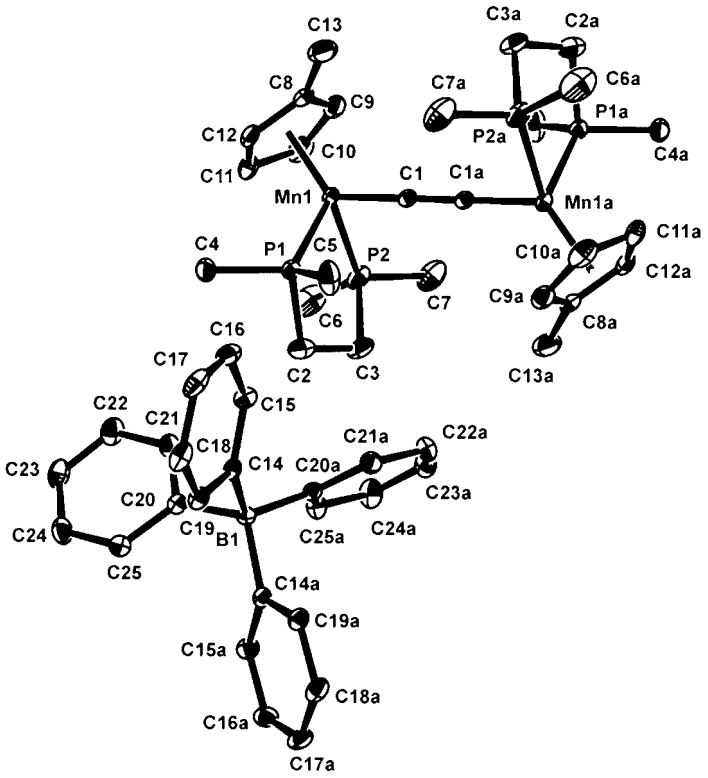

Figure 4. Molecular structure of [**1**][BPh_4] (30% probability displacement ellipsoids). Selected bond lengths [Å] and angles [°]: Mn1–C1 1.8003(18), C1–C1a 1.291(4), Mn1–MeCp(Cg) 2.165(2), Mn1–P1 2.2504(6) Mn1–P2 2.2201(6); Mn1-C1-C1a 178.2(2), C1-Mn1-P1 92.29(6), C1-Mn1-P2 88.48(6), P1-Mn1-P2 84.86(3). Hydrogen atoms are omitted for clarity.

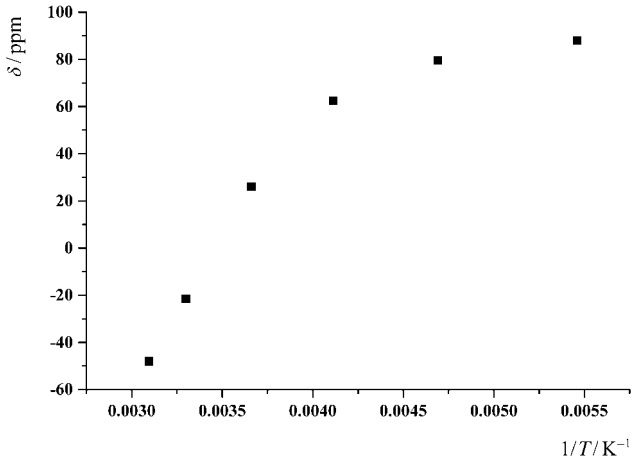

Figure 6. VT ^{31}P NMR chemical shift of **1**.

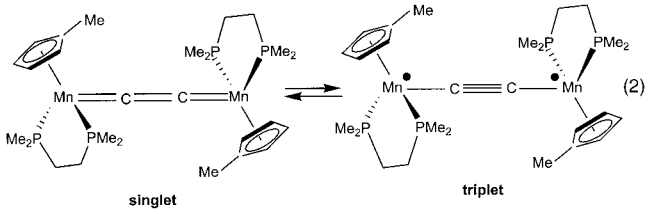

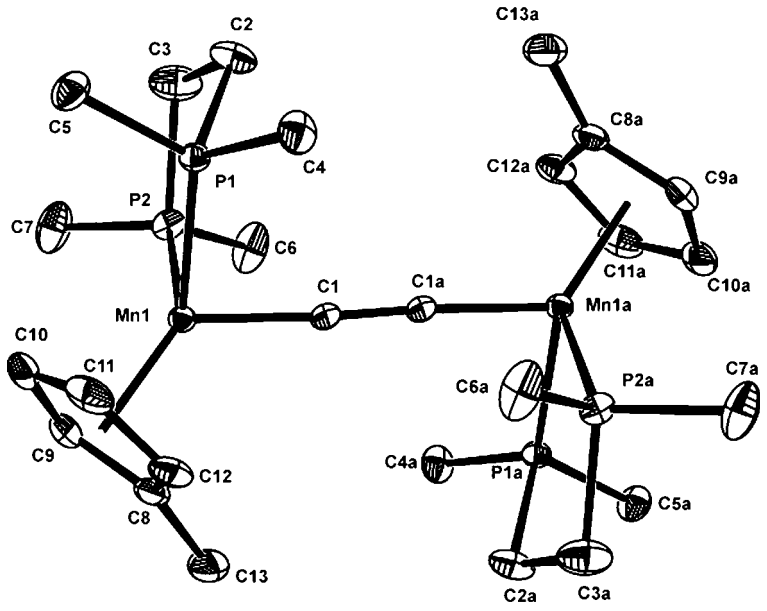

Figure 5. Molecular structure of **1** (30% probability displacement ellipsoids). Selected bond lengths [Å] and angles [°]: Mn1–C1 1.872(2), C1–C1a 1.271(4), Mn1–MeCp(Cg) 2.156(2), Mn1–P1 2.1871(7), Mn1–P2 2.1943(7); Mn1-C1-C1a 176.7(2), C1-Mn1-P1 87.62(7), C1-Mn1-P2 89.77(7), P1-Mn1-P2 83.66(2). Hydrogen atoms are omitted for clarity.

difference is nevertheless in contrast to the experimental observations. To put this in perspective one should bear in mind that the calculations were carried out on the model system **1-H**, since replacement of the phosphane methyl groups in **1** by H substituents[92b] might affect the relative energies of HOMO and LUMO, and therefore the energies of the triplet and singlet states. Nevertheless it is clear from the calculations that the singlet and triplet states are close in energy.

It was found that the minimum energies of the structures associated with the different electronic states refer to different rotamers of **1-H**, characterized by dihedral angles α of the pseudo mirror planes of the (MeC_5H_4)(dHpe)Mn fragments of 179.5° (*transoid* geometry) for the triplet state **T1** and for the singlet state **S1** and 89.9° (*gauche* geometry) for the other triplet state **T2**.

An analysis of MeC_5H_4 rotation was carried out on Mn–Mn rotamers. The respective energies of the rotational isomers of the C_5H_4Me rings are indicated in Figure 8. The calculated energy differences are rather small; therefore, the C_5H_4Me ring rotation is not considered further.

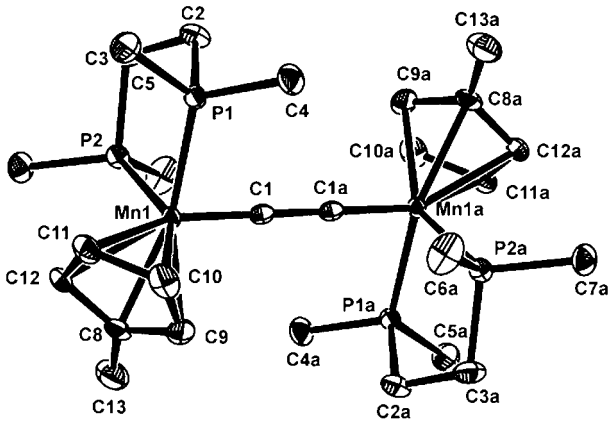

Figure 7. Molecular structure of [**1**][PF_6]$_2$ (30% probability displacement ellipsoids). Selected bond lengths [Å] and angles [°]: Mn1–C1 1.733(2), Mn1–MeCp(Cg) 2.164(2), Mn1–P1 2.2595(8), Mn1–P2 2.2818(7), C1–C1a 1.325(5); Mn1-C1-C1a 175.7(3), P1-Mn1-P2 85.28(3), P1-Mn1-C1 86.68(9), P2-Mn1-C1 94.59(8). Hydrogen atoms and the anions have been omitted for clarity.

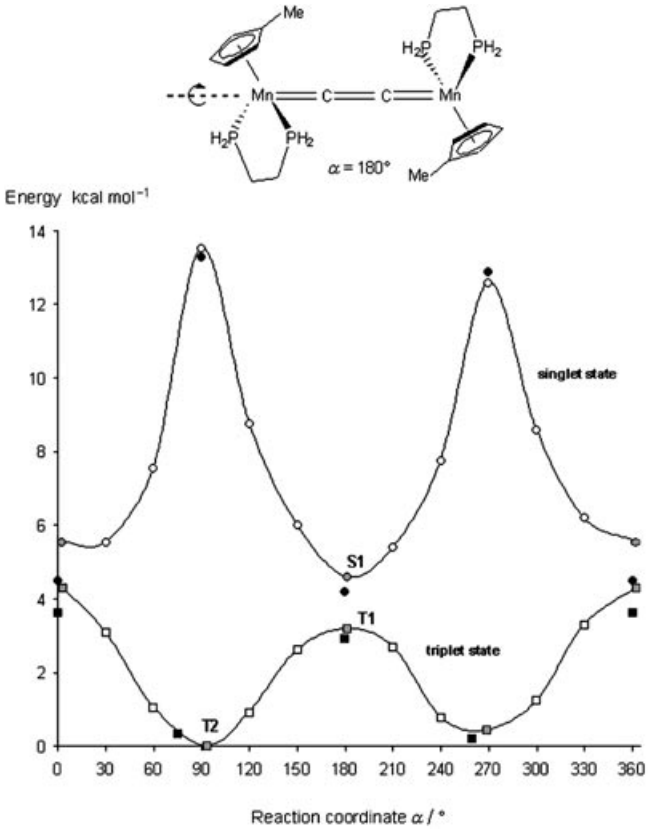

Figure 8. Potential energy surfaces for singlet and triplet states of model complex [(MeC_5H_4)(dHpe)MnC_2Mn(dHpe)(MeC_5H_4)] (**1-H**) showing the changes in relative energies with respect to the reaction coordinate α, defined as the dihedral angle between the local pseudo mirror planes of the two (MeC_5H_4)(dHpe)Mn fragments; distinct rotamers of the (MeC_5H_4) rings are also taken into account (open symbols: partially optimized geometry; gray symbols: fully optimized geometry for the (MeC_5H_4) ring with proximal methyl groups at 90° to the Mn–Mn axis; black symbols: fully optimized geometry for (MeC_5H_4) with distal methyl groups at 90° to the Mn–Mn axis.

The two potential-energy curves displayed in Figure 8 for the singlet and triplet states showed no crossing point along the reaction coordinate. The triplet state of model complex **1-H** is according to the calculations in all cases more stable than the singlet state, but very small energy differences of 1.3–1.4 kcal mol^{-1} are seen between the two states in the 0 and 180° conformations. It is also worth noting that the singlet state is considerably destabilized in its 90° (or 270°) geometry, and this results in a large gap of 13.5 kcal mol^{-1} with respect to the corresponding local triplet-state minima. It should be emphasized once more that the triplet curve being energetically below the singlet curve does not agree with the experimental observations and presumably corresponds to an artifact of the calculations. Nevertheless, the general rule that reactions with a barrier of 21 kcal mol^{-1} or less will proceed readily at room temperature[93a] suggests that facile rotation around the Mn–Mn vector can occur in solution regardless of the electronic configuration. A hint that the calculated order with **T2** ($\alpha = 90°$) energetically below **T1** and **S1** might not agree with reality comes from the structure determination of **1**, which suggests the real ground state geometry to have $\alpha = 180°$, which is the case for **T1** or **S1**. However, even **T1** lying energetically below **S1** seems to be false according to the NMR data and of the magnetic measurements. However, this situation should not be stressed too much, since **T1** and **S1** were computed to be very close and this allows one to conclude that both triplet and singlet states could be real and might even coexist with a very small energy difference.

A careful analysis of the frontier molecular orbitals of three prominent structures from the potential-energy surfaces is shown in Figure 9. The quantitative energy diagrams provide a comparison between the energy levels of selected frontier molecular orbitals of the **S1** molecule in its lowest energy conformation ($\alpha \approx 180°$) and the triplet state molecules **T1** ($\alpha \approx 180°$) and **T2** ($\alpha \approx 90°$). A relatively small energy gap of 0.29 eV separates the HOMO and LUMO of **S1**. These two perpendicular π orbitals have almost identical shapes. Due to the low symmetry of $CpML_2$ fragments[94] their $\pi_\perp$ and $\pi_\parallel$ orbitals are nondegenerate and in coplanar dinuclear arrangements ($\alpha = 0$ or 180°); this leads to nondegenerate $\pi_\perp$–$\pi_\perp$ and $\pi_\parallel$–$\pi_\parallel$ interactions. The HOMO and LUMO of the **S1** molecule are such a pair of $\pi_\perp$- and $\pi_\parallel$-derived π interactions delocalized along the Mn–C–C–Mn chain with Mn–C nodal planes.[93b] This situation in which one orbital of a closely related π set is unoccupied mirrors the fact that **1** is not an electron-precise molecule. The ion [**1**]$^{2-}$ would be so; this would require filling the LUMO of **1** with two electrons and the bridging C_2 unit to be an acetylide ligand C_2^{2-}. However, [**1**]$^{2-}$ seems energetically unfavorable, since the out-of-phase Mn–C interactions in the HOMO and LUMO of **S1** (or the two HOMOs of a hypothetical [**1**]$^{2-}$ ion) are reminiscent of the π-donor properties of the C_2^{2-} ligand, which pushes both these orbitals to quite high energies. The two "excess" electrons of [**1**]$^{2-}$ are therefore highly reducing in character. The CV results (vide infra) confirm this picture, in that reduction of **1** is just possible by one electron, and can occur only at very negative potentials that are presumably not even synthetically accom-

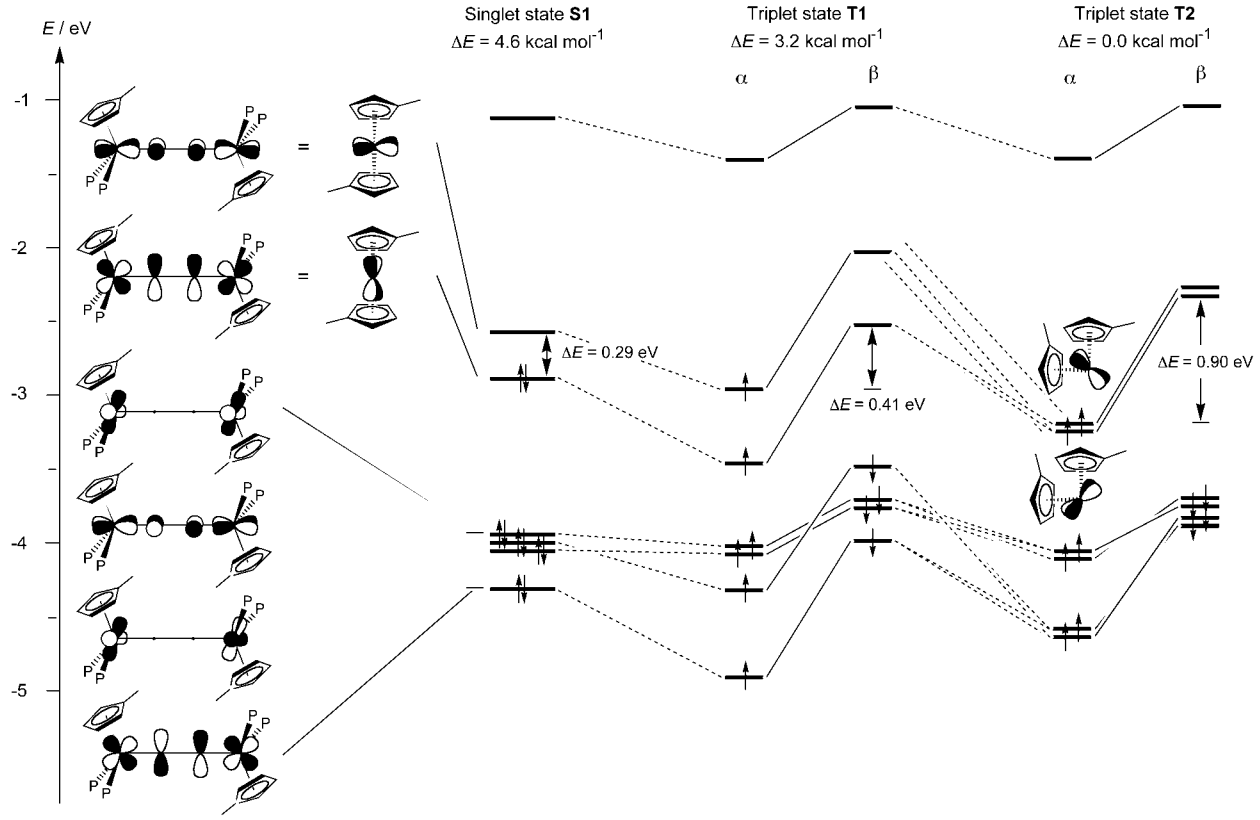

Figure 9. Energies of the main frontier orbitals for the selected molecules **S1**, **T1**, and **T2**.

plishable. It is a general feature of all the electronic states of **1** that their HOMOs and SOMOs are at very high absolute energies and therefore have relatively high values of the orbital coefficients at the Mn and C atoms. However, this enhances the electron-delocalization properties of molecules like **1** and also leads to their small work functions. Furthermore, the orbital diagram of **S1** shows a set of four occupied orbitals lying energetically below the HOMO, two of which exhibit practically only metal d character, whereas the other two are again a set of nondegenerate $\pi_\perp$ and $\pi_\parallel$ interactions with Mn–C bonding and C–C antibonding character. Overall the picture of the perpendicular π sets of the Mn–C_2–Mn fragments is reminiscent of the orbitals of two four-centered π systems, in which the two π_3 orbitals bear only two electrons and thus singlet- and triplet-type distributions result.

The triplet state in the geometry of **T1** ($\alpha \approx 180°$) then leads to a larger SOMO–LUMO separation than in **S1** (0.41 eV). The two unpaired electrons of like spin α occupy perpendicular orbitals of similar shape, which were HOMO and LUMO of **S1**, and the other filled orbitals of **T1** are also very similar to those of **S1**. The geometry of the triplet molecule **T2** with $\alpha = 90°$ shows a large increase in the SOMO–LUMO gap, which now amounts to 0.90 eV. In the spin-separated view the upper six singly occupied α spin orbitals can now form three doubly degenerate sets of $\pi_\perp$–$\pi_\parallel$ between the manganese centers, and the β orbitals accordingly can form two sets.

The spin-separated orbital picture reveals that the energy minima found for **T2**, **S1**, and **T1** are the result of counteraction of electron–electron repulsions and the extent of antibonding Mn–C interactions in the HOMO of **S1** with respect to the SOMOs of **T1** and **T2**. The energetic balancing of these factors with their small partial energy contributions leads to the observed quite small total energy differences of **S1**, **T1**, and **T2**. This indeed precludes qualitative arguments, and, if the calculational procedures tend to overestimate one or the other factor, then it is quite conceivable that they might not fully reproduce reality.

The described electronic behavior of complex **1** in solution, in which its singlet state may even be enforced and substantially lower in energy than the triplet state, was intended to be mimicked in the calculations by a general solvent effect, by using electrostatic model calculations, and furthermore by a specific solvent effect in which **1-H** is approached by a solvent molecule. Since **1** is a neutral species, the effect of model solvation applying electrostatic fields in the calculations was found to be minor and is therefore apparently not significant.

However, according to a Mulliken charge analysis for the **S1** molecule, the atoms of the carbon spacer carry a positive partial charge, whereas the metal centers have negative charges. Thus, a directed interaction between a solvent molecule, that is, THF with its electron-rich donor atom, and the carbon atoms could be expected. However, full geometry optimizations of model compound **1-H(THF)**, in which a tetrahydrofuran molecule interacts with one carbon atom of the C=C bridge, failed to converge for both spin states, apparently because steric repulsion was too large.

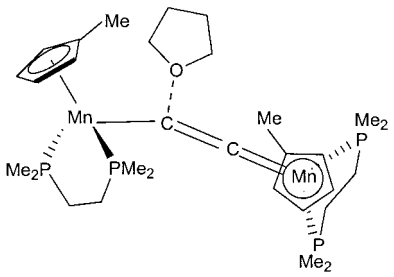

1-H(THF)

When the distance to THF was fixed at 2.6 Å, there was no clear-cut preference for a singlet or triplet ground state of the molecule, and the singlet structure was more stable by only 0.5 kcal mol^{-1}. This might indicate that electron-donating solvent molecules could induce a preference for the single state.

In conclusion, the gas-phase calculations suggested a triplet ground state of the neutral model complex $[(MeC_5H_4)(dHpe)MnC_2Mn(dHpe)(C_5H_4Me)]$ (**1-H**), which in fact might be artificial. Despite the inability to describe the kind of ground state with certainty by DFT calculations, these nevertheless made plausible the fact that the singlet/triplet energy gap for such dinuclear compounds can be very small, so that a singlet/triplet spin equilibrium is very likely to exist for **1**. In addition, the singlet state seems to be supported by solvent interactions.

Cyclic voltammetry (CV) studies, magnetic measurements, UV-visible studies, and vibrational spectroscopy of 1, [1][2], [1][PF$_6$], and [1][PF$_6$]$_2$: Complexes **1**, [**1**][**2**], [**1**][PF$_6$], and [**1**][PF$_6$]$_2$ exhibit structural variations that are directly related to the oxidation states of the manganese atoms. A similar behavior was observed in complexes with longer carbon chains between the metal centers.[43,44,48–59,67–74] According to the resonance forms of Equation (3) the Mn–C bonds shorten with increasing degree of oxidation, while the internal C–C bond elongates. This indicates that the cumulenic resonance form is transformed into the bis-carbyne type with a C–C single bond (Table 1).

$$Mn{=}C{=}C{=}Mn \leftrightarrow Mn{\equiv}C{-}C{\equiv}Mn \quad (3)$$

Table 1. Structural features [Å] of the Mn-C_2-Mn units in [**1**], [**1**]$^+$, and [**1**]$^{2+}$.

	Mn–C	C–C	C–Mn
1	1.872(2)	1.271(4)	1.872(2)
[**1**][PF$_6$]	1.792(3)	1.310(6)	1.792(3)
[**1**][BPh$_4$]	1.8003(18)	1.291(4)	1.8003(18)
[**1**][**2**]	1.817(7)	1.291(8)	1.760(6)
	1.774(6)	1.312(8)	1.776(6)
	1.780(6)	1.322(12)	1.780(6)
[**1**][PF$_6$]$_2$	1.733(2)	1.325(5)	1.733(2)

These structural features are expected to be reflected in appropriate physical properties of these complexes. For instance in Raman spectra symmetric a_{1g} stretching vibrations should appear as strong bands. Indeed the solid-state Raman spectrum of [**1**][PF$_6$] exhibits such an intense ν(C–C) band at 1564 cm^{-1} with a shoulder at 1590 cm^{-1}. A related characteristic strong band was also observed for [**1**][PF$_6$]$_2$ at 1314 cm^{-1}, but for **1** no such bands were detectable even when other wavelengths of the incident laser light were applied. The observed two-band pattern of [**1**][PF$_6$] could corroborate the existence of two rotamers. The emissions of [**1**]$^{2+}$ and [**1**]$^+$ indeed correspond to a_{1g} vibrations of the C_2 chain.[95–99] The observed shifts of the $\nu(C_2)$ band on going from [**1**]$^+$ to [**1**]$^{2+}$ indicate significant changes in the electronic configuration of the C_2 chain upon oxidation of the metal center(s) in the direction suggested by the above resonance forms. This behavior is typical of strongly electronically coupled systems. Similar structural features of the MnC_2Mn unit were detected in the $[\{Mn(dmpe)_2I\}_2(\mu\text{-}C_4)]^{n+}$ series ($n=0$, 1, 2).[67] In addition a Raman emission at around 340 cm^{-1} was assigned to the ν(Mn–C) vibration for all complexes,[100] and a band at around 270 cm^{-1} was attributed to an a_{1g} ν(Mn–P) stretch.[101] The IR spectra of **1**, [**1**][PF$_6$], and [**1**][PF$_6$]$_2$ revealed characteristic ν(C–C) vibrations for the methylcyclopentadienyl rings at 1629, 1689 (m), and 1644 cm^{-1} (w), respectively. The IR intensities of the ν(C=C) vibrations of the C_2 bridge were apparently too low to be observed.

The cyclic voltammogram starting from [**1**]$^{2+}$[PF$_6$]$_2$ (CV, 20 °C, NBu$_4$[PF$_6$]/CH$_3$CN, gold electrode, vs Fc/Fc$^+$) displays three fully reversible waves (Figure 10): at $E_{1/2}=-0.847$ V corresponding to the Mn^{III}–C_2–Mn^{III} [**1**]$^{2+}$[PF$_6$]$_2$/Mn^{II}–C_2–Mn^{III} [**1**]$^{2+}$[PF$_6$] redox couple ($\Delta E_p=0.060$ V and $i_{pa}/i_{pc}\approx 1$ for scan rates of 0.100–0.700 V s^{-1}), at $E_{1/2}=-1.835$ V due to the Mn^{III}–C_2–Mn^{II} [**1**]$^+$[PF$_6$]/Mn^{II}–C_2–Mn^{II} **1** couple, and at $E_{1/2}=-2.824$ V due to Mn^{III}–C_2–Mn^{II} **1**/Mn^{II}–C_2–Mn^{I} electron transfer. This species $[(MeC_5H_4)(dmpe)MnC_2Mn(dmpe)(MeC_5H_4)]^-$ is new and has not been generated in preparative studies. However, the potential of this redox couple may be too negative for reaching the anion by chemical means. The difference of the values of the first two waves ($\Delta E_{1/2}=0.988$ V) establishes a comproportionation constant of 8.6×10^{16} [$K_c=\exp(F\Delta E_{1/2}/RT)$].[6] Incidentally, both potential differences between the three redox processes have

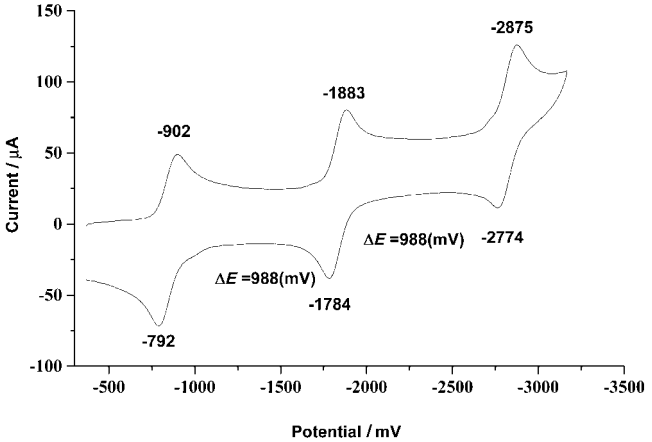

Figure 10. Cyclic voltammogram of [**1**][PF$_6$]$_2$ (10^{-3} M in CH$_3$CN nBu$_4$[PF$_6$]/THF, vs Fc/Fc$^+$, gold electrode, 100 mV s^{-1}).

the same large value, which emphasizes the existence of strong interactions between the manganese centers transmitted through the orbitals of the C_2 bridge. The K_c value of these complexes exceeds those of a series of complexes with a C_4 bridge $[\{Mn(dmpe)_2(X)\}_2(\mu\text{-}C_4)]^{n+}$ (X = I, 1.1×10^{10}; C≡CH, 7.5×10^{9}; C≡CSiMe$_3$, 2.2×10^{9}; C_4SiMe_3, 1.8×10)[60,67,93] by several orders of magnitude.

The temperature-dependent magnetic susceptibility was measured for **1** (Figure 11) and [**1**][PF_6] (Figure 12) in the

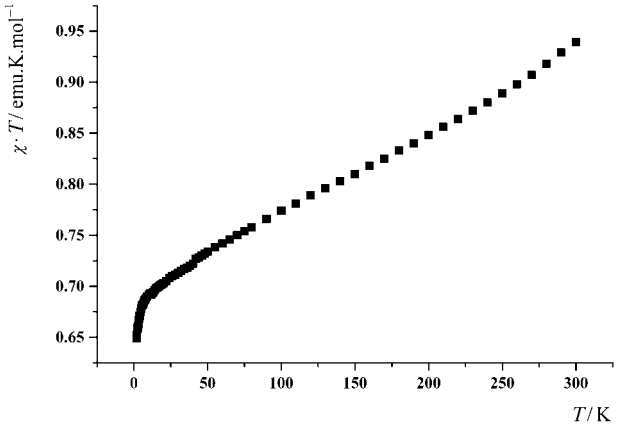

Figure 11. Temperature dependence of the molar magnetic susceptibility for **1**.

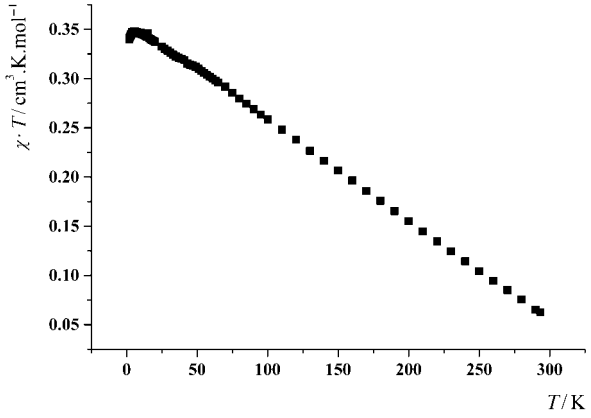

Figure 12. Temperature dependence of the molar magnetic susceptibility for [**1**]$^+$[PF_6].

solid state in the temperature range 2–300 K. Complex [**1**][PF_6] has a magnetic moment of 1.67 μ_B at 5 K and 1.04 μ_B at 200 K. This is a manifestation of its one-electron paramagnetism, as also suggested by the ^{1}H NMR studies.[43,48,67,87]

For **1** the χT value at 300 K drops from 0.94 emu K mol^{-1} (μ_{eff} = 2.47 μ_B) to 0.65 emu K mol^{-1} (μ_{eff} = 2.28 μ_B) at 2 K. From this we can conclude that for the **1** in the solid state the triplet state exists at all temperatures. However, the observed drop in magnetic moment at low temperatures is unexpected for a genuine paramagnet. This might be caused by antiferromagnetic coupling or by a singlet/triplet spin equilibrium with the singlet form as the ground state. The latter explanation is preferred, since DFT calculations on model molecules suggested the existence of singlet/triplet equilibria. Furthermore a spin equilibrium for solid **1** would parallel the observations found for this complex in solution, albeit with a significantly higher energetic preference for the singlet state in solution. Any respective quantification regarding the electronic states of **1** seemed to be theoretically and experimentally difficult both in solution and in the solid state.

The UV-visible spectra of the series of complexes **1**, [**1**]$^+$[PF_6], and [**1**]$^{2+}$[PF_6]$_2$ (Figure 13) are well-structured with an

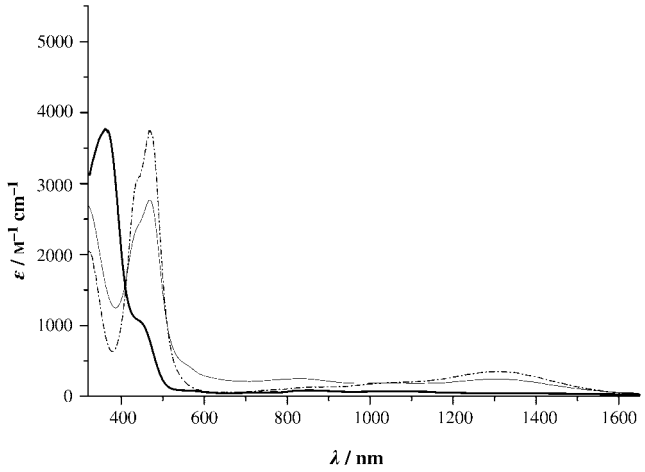

Figure 13. UV-visible spectra of **1**, [**1**]$^+$[PF_6] and [**1**]$^{2+}$[PF_6]$_2$ (CH_2Cl_2, ambient temperature, 1×10^{-4} M). $[\{C_5H_4CH_3Mn(dmpe)\}_2(\mu\text{-}C_2)]^{n+}$ —— $n=2$, —— $n=1$, ----- $n=0$.

intense band and a shoulder for all complexes and one additional band of low intensity at shorter wavelength for **1** and [**1**]$^+$[PF_6]. In comparison with the spectra of **1** and [**1**]$^{2+}$[PF_6]$_2$, [**1**]$^+$[PF_6] did not reveal an extra broad absorption at long wavelength that could be assigned to a mixed-valence band,[6,11,15,18,43,48,74,102–106] as expected for class II systems according to the Robin–Day classification. In accord with the CV results, this would allow one to conclude that the manganese end groups of **1**, [**1**]$^+$[PF_6], and [**1**]$^{2+}$[PF_6]$_2$ are electronically strongly coupled and that these complexes belong to class III. Furthermore, it is quite remarkable how strongly the systems are affected by charge, since the two major transitions, which are expected to arise from the same types of orbitals,[107] shift to shorter wavelengths on going from [**1**][PF_6] to [**1**][PF_6]$_2$. This is presumably due to the filled orbitals in the HOMO region of [**1**][PF_6], which are particularly sensitive to positive charge and are therefore significantly lowered in energy.

Conclusion

A series of half-sandwich Mn-C_2-Mn complexes of the type $[(MeC_5H_4)(dmpe)MnC_2Mn(dmpe)(C_5H_4Me)]^{n+}$ (n = 0, 1, 2) was prepared. In solution and in the solid state, it is assumed that the ground state of the neutral species **1** is diamagnetic, but a triplet state is in close energetic vicinity, so that **1** is

anticipated to exhibit the interesting phenomenon of a singlet/triplet equilibrium. Density functional calculations suggest a small energy gap between the two electronic states. Several types of physical studies on the dinuclear compounds stress the fact that the manganese centers have very strong electronic coupling according to class III systems of the Robin–Day classification. The interesting electronic properties exhibited by these complexes makes them promising candidates for the purpose of molecular electronics.

Experimental Section

General: Reagent-grade benzene, toluene, hexane, pentane, diethyl ether, and tetrahydrofuran were dried and distilled from sodium benzophenone ketyl prior to use. Dichloromethane was distilled first from P_2O_5, and then prior to use from CaH_2. Literature procedures were used to prepare the following compounds: 1,2-bis(dimethylphosphanyl)ethane (dmpe),[108] $[(MeC_5H_4)_2Mn]$,[85,86] $[(MeC_5H_4)_2Mn(dmpe)]$,[88] and $[(C_5H_5)_2Fe]^+[PF_6]^-$.[109] $Me_3SnC{\equiv}CSnMe_3$ was prepared by a modified literature procedure (see below). *n*BuLi (1.6 M in hexane), MeLi·LiBr (1.5 M in diethyl ether), and Me_3SnCl were used as received. All manipulations were carried out under a nitrogen atmosphere using Schlenk techniques or a dry box. IR spectra were obtained on a Bio-Rad FTS-45 instrument, and near-IR spectra on a Perkin–Elmer Lambda 19 UV-visible/near-IR spectrometer. NMR spectra were measured on a Varian Gemini-300 at 300 MHz for ^1H, 121.5 MHz for $^{31}P\{^1H\}$, and 282.3 MHz for ^{19}F. All NMR spectra of paramagnetic compounds were obtained from concentrated solutions of analytically pure samples. The assignment of the ^1H NMR signals for paramagnetic signals was principally based on the investigations of Köhler et al.[100,101] Chemical shifts for ^1H, ^{31}P, and ^{19}F are given in ppm with respect to the signals for residual solvent protons (^1H) of the deuterated solvents. $^{31}P\{^1H\}$ NMR spectra are referenced to 98% external H_3PO_4. Cyclic voltammograms were obtained with a BAS 100B/W instrument (10^{-3} M in 0.1 M $CH_3CN/nBu_4N[PF_6]$.

Preparation of $Me_3SnC{\equiv}CSnMe_3$: According to the literature procedure[110] acetylene (1 equiv) was introduced into a solution of *n*BuLi (2.1 equiv, 1.6 M) in hexane and diethyl ether at −70 °C under nitrogen. After stirring the resulting white suspension for 1 h at this temperature, Me_3SnCl (2.1 equiv) in diethyl ether was added, and the reaction mixture was stirred for 1 h at room temperature. Then a saturated solution of aqueous NH_4Cl was added carefully and slowly to the solution. The organic layer was separated and dried over magnesium sulfate overnight. Evaporation of the solvent gave pure $Me_3SnC{\equiv}CSnMe_3$ in good yield (70–80%) based on Me_3SnCl. Alternatively $Me_3SnC{\equiv}CSnMe_3$ can be prepared in good yield (80–90%) by treating $Me_3SiC{\equiv}CSiMe_3$ with MeLi·LiBr (2.2 equiv) in THF, followed by addition of Me_3SnCl (2.1 equiv) and stirring for 1 h at room temperature. A saturated solution of aqueous NH_4Cl was slowly added, and the organic layer was separated and dried over magnesium sulfate. Evaporation of the solvent gave pure $Me_3SnC{\equiv}CSnMe_3$ in good yield (70–80%) based on Me_3SnCl.

{Bis{[1,2-bis(dimethylphosphanyl)ethane](η⁵-methylcyclopentadienyl)-manganese(II/III)}(μ-CC)}·[tris(η²-methylcyclopentadienyl)manganate(II)] [1][2]: $[(MeC_5H_4)_2Mn(dmpe)]$ (363.4 mg, 1.00 mmol) was dissolved in THF (20 mL). $Me_3SnC{\equiv}CSnMe_3$ (88 mg, 0.25 mmol) in THF (10 mL) was added to the resulting yellow solution. The reaction mixture turned red and then dark red-brown. The mixture was stirred for 72 h. The dark red-brown solution was evaporated to dryness and washed with pentane, diethyl ether, and benzene until the washings were colorless. After extraction of the red-brown oily residue with THF (5 mL), the solution was filtered through Celite. Diethyl ether (15 mL) was added, and the mixture was stored at −30 °C. Red-brown crystals were obtained. Yield: 200 mg, 69%; elemental analysis calcd (%) for $C_{54}H_{67}Mn_3P_4$ (864.5): C 64.54, H 6.72; found: C 64.43, H 6.59; ^1H NMR ([D$_8$]THF, 300 MHz, 20 °C): $\delta =$ 27.8 (s, 18H, $(CH_3C_5H_4)_3Mn^-$), 1.1 (s, 6H; $CH_3C_5H_4$), −7.2 (s, 8H; $CH_3C_5H_4$), −8.2 ppm (br, 32H; dmpe); $^{31}P\{^1H\}$ NMR ([D$_8$]THF, 121.5 MHz, 40 °C): $\delta = 95.5$ ppm (s, dmpe); IR (KBr, 20 °C): $\tilde{\nu} = 1689$ (m, br), 1644 (w), 1592 (w), 1568 (w), 1531 (w), 1486 (w) ν(C=C), 1449 (w), 1417 (m), 1377 (w), 1294 (w), 1278 (m), 1233 (w), 1178 (w, br), 1126 (m), 1081 (w), 1058 (w), 1027 (s), 938 cm^{-1} (s).

Complex [1]⁺[PF₆]: $[(MeC_5H_4)_2Mn(dmpe)]$ (363.4 mg, 1.00 mmol) was dissolved in THF (20 mL). $Me_3SnC{\equiv}CSnMe_3$ (88 mg, 0.25 mmol) in THF (10 mL) was added to the resulting yellow solution. The reaction mixture turned red and then dark red-brown. The mixture was stirred for 72 h. After addition of $K[PF_6]$ (500 mg, 2.72 mmol) and stirring for 24 h the dark red-brown solution was evaporated to dryness and washed with pentane and diethyl ether until the washings were colorless. After extraction of the brown solid residue with dichloromethane (5 mL), the solution was filtered through Celite. Diethyl ether (15 mL) was added and the mixture was stored at −30 °C. Black-brown crystals were obtained. Yield: 195 mg, 80%; elemental analysis calcd (%) for $C_{26}H_{46}F_6Mn_2P_5$ (737.3): C 42.35, H 6.29; found: C 42.71, H 6.52; ^1H NMR (CD_2Cl_2, 300 MHz, 20 °C): $\delta = 0.3$ (s, 6H; $CH_3C_5H_4$), −7.9 (br, 40H; $CH_3C_5H_4$ and dmpe), −8.2 ppm (br, 32H; dmpe); $^{31}P\{^1H\}$ NMR (CD_2Cl_2, 121.5 MHz, 20 °C): $\delta = -145.7$ ppm (sept, $J_{PF} = 719$ Hz, $[PF_6]^-$); IR (KBr, 20 °C): $\tilde{\nu} = 1629$ (w, br), 1487 (w; C=C), 1454 (w), 1418 (m), 1375 (w), 1298 (w), 1280 (m), 1264 (w), 1236 (w), 1127 (m), 1080 (w), 1032 (w), 946 (s), 933 (s; C–P), 841 cm^{-1} (vs; P–F); $\mu_{eff} = 1.04$ (220), 1.44 (100), 1.67 μ_B (5 K).

Complex [1]⁺[BPh₄]: $[(MeC_5H_4)_2Mn(dmpe)]$ (363.4 mg, 1.00 mmol) was dissolved in THF (20 mL). $Me_3SnC{\equiv}CSnMe_3$ (88 mg, 0.25 mmol) in THF (10 mL) was added to the resulting yellow solution. The reaction mixture turned red and then dark red-brown. The mixture was stirred for 72 h. After addition of $Na[BPh_4]$ (924 mg, 2.7 mmol) and stirring for 24 h, the dark red-brown solution was evaporated to dryness and washed with pentane and diethyl ether until the wash solution was colorless. After extraction of the red-brown solid residue with dichloromethane (5 mL), the solution was filtered through Celite. Diethyl ether (15 mL) was added and the mixture was stored at −30 °C. Red-brown crystals were obtained. Yield: 185 mg, 60.6%. Alternatively this complex can be obtained in 90% yield by reaction of $[\mathbf{1}]^+[PF_6]$ and $Na[BPh_4]$ (1 equiv) in THF. Yield (90%); elemental analysis calcd (%) for $C_{50}H_{66}BMn_2P_4$ (911.41): C 65.87, H 7.30; found: C 66.00, H 7.50; ^1H NMR (CD_2Cl_2, 300 MHz, 25 °C): $\delta =$ 7.4 (br, 8H; *o*-C_6H_5), 7.1 (br, 8H; *m*-C_6H_5), 6.9 (br, 4H; *p*-C_6H_5), 0.3 (br, 6H; $CH_3C_5H_4$), −6.7 ppm (br, 40H; $CH_3C_5H_4$ and dmpe). $^{31}P\{^1H\}$ NMR (CD_2Cl_2, 121.5 MHz, 25 °C): $\delta = 48.6$ ppm (s, dmpe); $^{13}C\{^1H\}$ NMR (CD_2Cl_2, 125 MHz, 25 °C): $\delta = 122.7$ (s, *p*-C_6H_5), 126.9 (s, *o*-C_6H_5), 137.2 (s, *m*-C_6H_5), 165.8 ppm (q, $^1J_{B,C} = 50$ Hz, BC_6H_5); IR (KBr, 20 °C): $\tilde{\nu} =$ 1935 (vw), 1874 (vw), 1813 (vw), 938 cm^{-1} (s; C–P).

{Bis{[1,2-bis(dimethylphosphanyl)ethane](η⁵-methylcyclopentadienyl)-manganese(III/III)}(μ-CC)} bis(hexafluorophosphate) [1]²⁺[PF₆]₂: A solution of $[(C_5H_5)_2Fe][PF_6]$ (33.1 mg, 0.1 mmol) in CH_2Cl_2 (10 mL) was added at room temperature to a solution of $[\mathbf{1}]^+[PF_6]$ (73.7 mg, 0.1 mmol) in CH_2Cl_2 (10 mL) and stirred overnight. After evaporation of the solvent to 2 mL, diethyl ether (20 mL) was added. A dark brown precipitate was obtained, which was washed several times with diethyl ether until the washings were colorless. Recrystallization from MeCN/diethyl ether gave $[\mathbf{1}]^{2+}[PF_6]_2$. Yield: 84 mg, 95%; elemental analysis calcd (%) for $C_{26}H_{46}F_{12}Mn_2P_6$: C 35.39, H 5.26; found: C 35.73, H 5.04. ^1H NMR (CD_3NO_2, 300 MHz, 30 °C): $\delta = 0.96$ (s, 24H; $P(CH_3)_2$), 1.4 (s, 8H; PCH_2), 2.1 (s, 6H; $CH_3C_5H_4$), 6.2 ppm (br, 8H; $CH_3C_5H_4$); $^{31}P\{^1H\}$ NMR (CD_3NO_2, 121.5 MHz, 40 °C): $\delta = 79.3$ (br s, dmpe), −144.8 ppm (sept, $^1J_{P,F} = 715$ Hz; PF_6); $^{13}C\{^1H\}$ NMR (CD_3NO_2, 125 MHz, 40 °C): $\delta =$ 14.6 ppm (br; dmpe), 94.0 (s; MeCp); ^{19}F NMR (CD_3NO_2, 282.3 MHz, 30 °C): $\delta = -74.1$ ppm (d, $^1J_{F,P} = 714$ Hz; PF_6). IR (KBr, 20 °C): $\tilde{\nu} = 2012$ (w; C=C), 1638 (br, w), 1580 (br, w; C=C), 939 (s; C–P), 835 cm^{-1} (vs, br; P–F).

{Bis{[1,2-bis(dimethylphosphanyl)ethane](η⁵-methylcyclopentadienyl)-manganese(I)}(μ-CC)} (1): $[\mathbf{1}]^+[PF_6]$ (73.7 mg, 0.1 mmol) in THF (20 mL) was treated with Na/Hg (5% Na) in THF and stirred for 4 h. After filtration through Celite and evaporation of the solvent, the brown crude residue was extracted with pentane (3×5 mL) and was filtered again through Celite. Concentration of the solution and crystallization at −40 °C gave deep red crystals of **1**. Yield: 48 mg, 81%; elemental analysis calcd (%) for $C_{26}H_{46}Mn_2P_4$: C 52.71, H 7.83; found: C 52.80, H 7.52; ^1H NMR ([D$_8$]toluene, 300 MHz, 20 °C): $\delta = 6.67$ (s, 4H; $CH_3C_5H_4$), 4.95 (s, 4H; $CH_3C_5H_4$), 2.39 (s, 6H; $CH_3C_5H_4$), 1.54 (s, 4H; PCH_2), 0.44 (s, 4H; PCH_2), 0.10 (s, 12H; PCH_3), −0.09 ppm (s, 12H; PCH_3); ^{31}P NMR ([D$_8$]toluene, 125 MHz, 30 °C): $\delta = -21.6$ (s; dmpe); IR (KBr, 20 °C): $\tilde{\nu} =$

1805 (w), 1626 (br, m), 1487 (w), 1450 (w), 1417 (m), 1378 (w), 932 cm^{-1} (s; C–P); μ_{eff} = 2.74 (300), 2.61 (200), 2.49 (100), 2.35 (10), 2.28 μ_B (2 K).

{Bis{[1,2-bis(dimethylphosphanyl)ethane](η⁵-methylcyclopentadienyl)manganese(I/I)}[μ-(1,2-bis(dimethylphosphanyl)ethane)]} (3): $[(MeC_5H_4)_2Mn(dmpe)]$ (363.4 mg, 1.00 mmol) was dissolved in THF (20 mL). $Me_3SnC{\equiv}CSnMe_3$ (88 mg, 0.25 mmol) in THF (10 mL) was added to the resulting yellow solution. The reaction mixture turned red and then dark red-brown. The mixture was stirred for 72 h. The dark red-brown solution was evaporated to dryness, and the residue extracted with pentane and diethyl ether. The solvent was evaporated to yield compound **3**. Compound **3** was crystallized from diethyl ether at −30 °C. Yield: 15 mg, 18 %; elemental analysis calcd (%) for $C_{30}H_{62}Mn_2P_6$: C 50.15, H 8.70; found: C 50.52, H 8.60; ^{1}H NMR (C_6D_6, 300 MHz, 30 °C): δ = 3.6, 3.8 (s, 8H; $CH_3C_5H_4$), 2.2 (s, 6H; $CH_3C_5H_4$), 1.1, 1.2, 1.3, 1.7 ppm (s, 48H; dmpe and μ-dmpe); $^{31}P\{^1H\}$ NMR (C_6D_6, 125 MHz, 30 °C): δ = 56.0 (s, μ-dmpe), 87.9 ppm (s; dmpe); $^{13}C\{^1H\}$ NMR (C_6D_6, 125 MHz, 25 °C): δ = 83.6 (s; *ipso*-C, $CH_3C_5H_4$), 75.9 (s; $CH_3C_5H_4$), 71.5 (s; $CH_3C_5H_4$), 70.7 (s; $CH_3C_5H_4$), 34.1 (m; PCH_2), 32.4 (t, $J_{C,P}$ = 20.6 Hz; PCH_3), 25.4 (m; PCH_2), 24.9 (t, $J_{C,P}$ = 7 Hz; μ-PCH_3), 23.9 (t, $J_{C,P}$ = 7 Hz; PCH_3), 22.6 (d, $J_{C,P}$ = 15 Hz; μ-PCH_2), 21.9 (d, $J_{C,P}$ = 14 Hz; PCH_2), 15.2 ppm (s, $CH_3C_5H_4$).

X-ray crystal structure analyses: X-ray diffraction data were collected at 183(1) K for compounds $[(\eta^5,\eta^2\text{-}MeC_5H_4)_2Mn(dmpe)]$, **3**, [**1**][**2**], [**1**][BPh_4], [**1**][PF_6], [**1**][PF_6]$_2$, and **1**, by using an imaging plate detector system (Stoe IPDS) with graphite-monochromated $Mo_{K\alpha}$ radiation. A total of 149, 167, 210, 263, 210, 164, and 167 images were exposed at constant times of 5.00, 1.50, 8.00, 3.00, 1.80, 3.60, and 2.00 min per image for the seven structures, respectively. The crystal-to-image distances were set to 54, 50, 70, 50, 50, 50, and 50 mm (θ_{max} range: 25.90° for [**1**][**2**] and 30.40° for [**1**][PF_6]). φ rotation (for **1**, [**1**][PF_6], and **3**) and oscillation modes for the other four compounds were used for the increments of 1.2, 1.0, 1.2° and 1.3, 1.0, 0.8, and 1.4° per exposure in each case. Total exposure times were 24, 16, 43, 32, 16, 21, and 17 h. The intensities were integrated by using a dynamic peak profile analysis, and an estimated mosaic spread (EMS) check was performed to prevent overlapping intensities. For the cell parameter refinements 7997 to 8000 reflections were selected from the whole limiting spheres with intensities $I > 6\sigma(I)$ for all structures. A total of 19988, 41387, 56773, 27350, 20631, 12387, and 17389 reflections were collected, of which 5161, 10544, 24864, 7737, 4685, 4993, and 4440 were unique after data reduction (R_{int} = 0.0719, 0.0452, 0.1543, 0.0631, 0.1046, 0.0554, and 0.0431). For the numerical absorption corrections[120] 12, 25, 10, 11, 11, 12, and 19 indexed crystal faces were used.

All crystals were embedded in polybutene oil in a glove box. The crystal quality was then examined by using a polarizing microscope. Sometimes,

Table 2. Crystallograhic details of $[(\eta^5\text{-}MeC_5H_4)(\eta^2\text{-}MeC_5H_4)Mn(dmpe)]$, **3**, [**1**][**2**], [**1**][BPh_4], **1**, and [**1**][PF_6]$_2$.

	$[(\eta^5,\eta^2\text{-}MeC_5H_4)_2Mn(dmpe)]$	**3**	[**1**][**2**]
formula	$C_{18}H_{30}MnP_2$	$C_{30}H_{62}Mn2P_6$	$C_{132}H_{201}Mn_9P_{12}$
color, habit	light green plate	orange block	red plate
M_r	363.30	718.50	2654.02
crystal size [mm]	0.06 × 0.20 × 0.28	0.56 × 0.55 × 0.37	0.15 × 0.25 × 0.31
T [K]	183(2)	183(2)	183(2)
$\lambda(Mo_{K\alpha})$ [Å]	0.71073	0.71073	0.71073
crystal system	monoclinic	monoclinic	triclinic
space group	$P2_1/n$	$P2_1/c$	$P\bar{1}$
a [Å]	8.5805(5)	16.2679(9)	16.3581(11)
b [Å]	15.3024(12)	14.2086(10)	20.6494(14)
c [Å]	14.8060(8)	17.2417(10)	23.6425(16)
α [°]	90	90	112.426(8)
β [°]	95.771(7)	115.763(6)	107.625(8)
γ [°]	90	90	93.828(8)
V [Å^3]	1934.2(2)	3589.2(4)	6883.4(8)
Z	4	4	2
ρ_{calcd} [g cm^{-3}]	1.248	1.330	1.281
μ [mm^{-1}]	0.841	0.990	0.980
F(000)	772	1528	2796
transmission range	0.9513–0.7986	0.7264–0.6545	0.8709–0.7589
θ range [°]	5.26 < 2θ > 58.70	5.80 < 2θ > 60.60	3.9 < 2θ > 51.8
measured reflections	19988	41837	56773
unique reflections	5161	10544	24864
$I > 2\sigma(I)$ reflections	2817	6818	6179
parameters	196	357	1352
GOF (for F^2)	0.874	1.027	0.558
R_1 [$I > 2\sigma(I)$]/R_1 (all data)[a]	0.0301/0.0745	0.0399/0.0688	0.0498/0.2056
wR_2 [$I > 2\sigma(I)$]/wR_2 (all data)[a]	0.0442/0.0483	0.1068/0.1286	0.0768/0.1085
$\Delta\rho_{max/min}$	0.298/−0.370	1.014/−1.472	1.282/−0.400
	[**1**][BPh_4]	**1**	[**1**]$^{2+}$[PF_6]$_2$
formula	$C_{54}H_{74}BMn_2OP_4$	$C_{26}H_{46}Mn_2P_4$	$C_{26}H_{46}F_{12}Mn_2P_6$
color, habit	red plate	red block	red-orange plate
M_r	983.70	592.39	882.33
crystal size [mm]	0.06 × 0.18 × 0.30	0.24 × 0.30 × 0.32	0.07 × 0.15 × 0.19
T [K]	183(2)	183(2)	183(2)
$\lambda(Mo_{K\alpha})$ [Å]	0.71073	0.71073	0.71073
crystal system	monoclinic	monoclinic	triclinic
space group	$I2/a$	$P2_1/n$	$P\bar{1}$
a [Å]	15.3746(7)	9.1696(7)	8.2777(7)
b [Å]	13.7405(6)	16.6636(9)	9.4492(9)
c [Å]	25.1942(11)	9.9733(8)	12.1706(11)
α [°]	90	90	79.031(11)
β [°]	102.277(5)	100.309(9)	78.057(10)
γ [°]	90	90	89.678(10)
V [Å^3]	5200.7(4)	1499.31(18)	913.77(14)
Z	4	2	1
ρ_{calcd} [g cm^{-3}]	1.256	1.312	1.603
μ [mm^{-1}]	0.645	1.068	1.034
F(000)	2084	624	450
transmission range	0.8828–0.5867	0.7962–0.7150	0.9369–0.8644
θ range [°]	5.6 < 2θ > 60.60	6.10 < 2θ > 60.50	5.5 < 2θ > 60.70
measured reflections	27350	17389	12387
unique reflections	7737	4440	4993
$I > 2\sigma(I)$ reflections	4267	2971	3311
parameters	283	150	213
GOF (for F^2)	0.996	1.038	1.006
R_1 [$I > 2\sigma(I)$]/R_1 (all data)[a]	0.0401/0.0898	0.0365/0.0624	0.0364/0.0662
wR_2 [$I > 2\sigma(I)$]/wR_2 (all data)[a]	0.0704/0.0764	0.0871/0.0977	0.0779/0.0930
$\Delta\rho_{max/min}$	0.526/−0.519	1.368/−0.592	0.726/−1.059

[a] $R_1 = \Sigma(F_o - F_c)/\Sigma F_o$; $wR_2 = [\Sigma w(F_o^2 - F_c^2)^2/\Sigma w(F_o^2)^2]^{1/2}$.

crystals with intrusions (holes or solvent) or with tiny intergrown pieces had to be accepted for the X-ray experiment. Cutting crystals to a suitable size is always a procedure that can damage a crystal of good quality because of different cleavage properties. Twins can be generated during handling. In general, the structures were solved with an incomplete data set (50% or less completeness) while the measurement was still being performed, because the correct chemical formula cannot always be predicted when solvent molecules (e.g., for [**1**][BPh_4]) co-crystallize with the complex, or, as in the case of [**1**][**2**], a mixture of different complexes was found (ratio 3:4 in the asymmetric unit of the cell, $Z'=7$). The corrected formula was then used for the final absorption correction. All these procedures were calculated by using the Stoe IPDS software.[111] The measurement temperatures were controlled by an Oxford cryogenic system.

The structures were solved with the merged unique data set after checking for correct space groups. The Patterson method was used to solve the crystal structures by applying the software options of the program SHELXS-97.[112] The structure refinements were performed with the program SHELXL-97.[113] The programs PLATON[114] and PLUTON[115] were used to check the results of the X-ray analyses; they are helpful for the interpretation of the initially determined structural models. They were also used for the completion of the structure by checking the difference electron density calculations. Relevant crystallographic data are collected in Table 2. All seven structures crystallize in centrosymmetric space groups.

CCDC 218719–218725 contain the supplementary crystallographic data for this paper. These data can be obtained free of charge via www.ccdc.cam.ac.uk/conts/retrieving.html (or from the Cambridge Crystallographic Data Centre, 12 Union Road, Cambridge CB21EZ, UK; fax: (+44) 1223-336-033; or deposit@ccdc.cam.uk).

Computational details: DFT calculations were performed with the TURBOMOLE program package, version 5.5.[116] The Vosko–Wilk–Nusair[117] local density approximation (LDA) and the generalized gradient approximation (GGA) with corrections for exchange and correlation according to Becke[118] and Perdew[119] (BP86) were used for all calculations. The TURBOMOLE approach to DFT GGA calculations is based on the use of Gaussian-type orbitals (GTO) as basis functions. Geometries were pre-optimized within the framework of the RI-*J* approximation[120] using accurate triple-ζ valence basis sets augmented by one polarization function TZV(P)[121a] for Mn and P, and slightly smaller polarized split-valence SV(P)[121b] basis sets of double-ζ size for the remaining elements. In the final steps of the geometry optimizations, all elements were treated with the accurate TZV(P) basis sets. The geometry optimizations, managed mainly through the use of the modules RIDFT, RDGRAD, and RELAX supplied with the TURBOMOLE program package, were considered converged when the change in total energy was less than 10^{-6} Hartree and the norm of the Cartesian gradient was smaller than 10^{-3} (fully optimized geometry) or 5.10^{-3} Hartree Å^{-1} (constrained geometries).

Acknowledgments

Funding from the Swiss National Science Foundation (SNSF) and from the University of Zürich is gratefully acknowledged.

[1] F. Paul, C. Lapinte, *Coord. Chem. Rev.* **1998**, *180*, 431–509.
[2] J. M. Tour, *Acc. Chem. Res.* **2000**, *33*, 791–804.
[3] M. D. Ward, *Chem. Soc. Rev.* **1995**, *24*, 121–134.
[4] M. D. Ward, *Chem. Ind.* **1996**, 568–573.
[5] A. Harriman, R. Ziessel, *Coord. Chem. Rev.* **1998**, *171*, 331–339.
[6] C. Creutz, *Prog. Inorg. Chem.* **1983**, *30*, 1–73.
[7] K. Sonogashira, S. Takahashi, N. Hagihara, *Macromolecules* **1977**, *10*, 879–880.
[8] K. Sonogashira, Y. Fujikura, T. Yatake, N. Toyoshima, S. Takahashi, N. Hagihara, *J. Organomet. Chem.* **1978**, *145*, 101–108.
[9] M. Carano, M. Careri, F. Cicogna, I. D'Ambra, J. L. Houben, G. Ingrosso, M. Marcaccio, F. Paolucci, C. Pinzino, S. Roffia, *Organometallics* **2001**, *20*, 3478–3490.
[10] S. Chakraborty, R. H. Laye, P. Munshi, R. L. Paul, M. D. Ward, G. K. Lahiri, *J. Chem. Soc. Dalton Trans.* **2002**, 2348–2353.
[11] N. Chanda, R. H. Laye, S. Chakraborty, R. L. Paul, J. C. Jeffrey, M. D. Ward, G. K. Lahiri, *J. Chem. Soc. Dalton Trans.* **2002**, 3496–3504.
[12] M. J. Crossley, L. A. Johnston, *Chem. Commun.* **2002**, 1122–1123.
[13] F. J. Fernandez, M. Alfonso, H. W. Schmalle, H. Berke, *Organometallics* **2001**, *20*, 3122–3131.
[14] V. Grosshenny, A. Harriman, R. Ziessel, *Angew. Chem.* **1995**, *107*, 2921–2025; *Angew. Chem. Int. Ed. Engl.* **1995**, *34*, 2705–2708.
[15] N. C. Harden, E. R. Humphrey, J. C. Jeffrey, S. M. Lee, M. Marcaccio, J. A. McCleverty, L. H. Rees, M. D. Ward, *J. Chem. Soc. Dalton Trans.* **1999**, 2417–2426.
[16] L. Jones, J. S. Schumm, J. M. Tour, *J. Org. Chem.* **1997**, *62*, 1388–1410.
[17] M. Kemp, V. Mujica, M. A. Ratner, *J. Chem. Phys.* **1994**, *101*, 5172–5178.
[18] R. H. Laye, S. M. Couchman, M. D. Ward, *Inorg. Chem.* **2001**, *40*, 4089–4092.
[19] S. Le Stang, F. Paul, C. Lapinte, *Organometallics* **2000**, *19*, 1035–1043.
[20] V. Mujica, M. Kemp, M. A. Ratner, *J. Chem. Phys.* **1994**, *101*, 6856–6864.
[21] V. Mujica, M. Kemp, M. A. Ratner, *J. Chem. Phys.* **1994**, *101*, 6849–6855.
[22] G. Pourtois, D. Beljonne, J. Cornil, M. A. Ratner, J. L. Bredas, *J. Am. Chem. Soc.* **2002**, *124*, 4436–4447.
[23] S. Richeter, C. Jeandon, J. P. Gisselbrecht, R. Ruppert, H. J. Callot, *J. Am. Chem. Soc.* **2002**, *124*, 6168–6179.
[24] M. P. Samanta, W. Tian, S. Datta, J. I. Henderson, C. P. Kubiak, *Phys. Rev. B* **1996**, *53*, R7626–R7629.
[25] K. Sendt, L. A. Johnston, W. A. Hough, M. J. Crossley, N. S. Hush, J. R. Reimers, *J. Am. Chem. Soc.* **2002**, *124*, 9299–9309.
[26] M. Shiotsuka, Y. Yamamoto, S. Okuno, M. Kitou, K. Nozaki, S. Onaka, *Chem. Commun.* **2002**, 590–591.
[27] J. M. Tour, L. Jones, D. L. Pearson, J. J. S. Lamba, T. P. Burgin, G. M. Whitesides, D. L. Allara, A. N. Parikh, S. V. Atre, *J. Am. Chem. Soc.* **1995**, *117*, 9529–9534.
[28] J. M. Tour, A. M. Rawlett, M. Kozaki, Y. X. Yao, R. C. Jagessar, S. M. Dirk, D. W. Price, M. A. Reed, C. W. Zhou, J. Chen, W. Y. Wang, I. Campbell, *Chem. Eur. J.* **2001**, *7*, 5118–5134.
[29] J. H. K. Yip, J. G. Wu, K. Y. Wong, K. P. Ho, C. S. N. Pun, J. J. Vittal, *Organometallics* **2002**, *21*, 5292–5300.
[30] J. H. K. Yip, J. G. Wu, K. Y. Wong, K. W. Yeung, J. J. Vittal, *Organometallics* **2002**, *21*, 1612–1621.
[31] K. T. Wong, J. M. Lehn, S. M. Peng, G. H. Lee, *Chem. Commun.* **2000**, 2259–2260.
[32] C. P. Collier, J. O. Jeppesen, Y. Luo, J. Perkins, E. W. Wong, J. R. Heath, J. F. Stoddart, *J. Am. Chem. Soc.* **2001**, *123*, 12632–12641.
[33] M. I. Bruce, B. G. Ellis, B. W. Skelton, A. H. White, *J. Organomet. Chem.* **2000**, *607*, 137–145.
[34] J. M. Tour, M. Kozaki, J. M. Seminario, *J. Am. Chem. Soc.* **1998**, *120*, 8486–8493.
[35] M. A. Reed, C. Zhou, C. J. Muller, T. P. Burgin, J. M. Tour, *Science* **1997**, *278*, 252–254.
[36] D. L. Pearson, L. Jones, J. S. Schumm, J. M. Tour, *Synth. Met.* **1997**, *84*, 303–306.
[37] C. P. Collier, E. W. Wong, M. Belohradsky, F. M. Raymo, J. F. Stoddart, P. J. Kuekes, R. S. Williams, J. R. Heath, *Science* **1999**, *285*, 391–394.
[38] A. R. Pease, J. O. Jeppesen, J. F. Stoddart, Y. Luo, C. P. Collier, J. R. Heath, *Acc. Chem. Res.* **2001**, *34*, 433–444.
[39] M. Akita, M. C. Chung, A. Sakurai, S. Sugimoto, M. Terada, M. Tanaka, Y. Morooka, *Organometallics* **1997**, *16*, 4882–4888.
[40] M. A. S. Aquino, F. L. Lee, E. J. Gabe, C. Bensimon, J. E. Greedan, R. J. Crutchley, *J. Am. Chem. Soc.* **1992**, *114*, 5130–5140.
[41] M. H. Baik, T. Ziegler, C. K. Schauer, *J. Am. Chem. Soc.* **2000**, *122*, 9143–9154.
[42] F. Barigelletti, L. Flamigni, V. Balzani, J. P. Collin, J. P. Sauvage, A. Sour, E. C. Constable, A. M. W. C. Thompson, *J. Am. Chem. Soc.* **1994**, *116*, 7692–7699.

[43] T. Bartik, B. Bartik, M. Brady, R. Dembinski, J. A. Gladysz, *Angew. Chem.* **1996**, *108*, 467–469; *Angew. Chem. Int. Ed. Engl.* **1996**, *35*, 414–417.
[44] T. Bartik, W. Q. Weng, J. A. Ramsden, S. Szafert, S. B. Falloon, A. M. Arif, J. A. Gladysz, *J. Am. Chem. Soc.* **1998**, *120*, 11071–11081.
[45] A. C. Benniston, A. Harriman, V. Grosshenny, R. Ziessel, *New J. Chem.* **1997**, *21*, 405–408.
[46] A. C. Benniston, V. Goulle, A. Harriman, J. M. Lehn, B. Marczinke, *J. Phys. Chem.* **1994**, *98*, 7798–7804.
[47] M. Beley, S. Chodorowskikimmes, J. P. Collin, P. Laine, J. P. Launay, J. P. Sauvage, *Angew. Chem.* **1994**, *106*, 1854–1856; *Angew. Chem. Int. Ed. Engl.* **1994**, *33*, 1775–1778.
[48] M. Brady, W. Q. Weng, Y. L. Zhou, J. W. Seyler, A. J. Amoroso, A. M. Arif, M. Bohme, G. Frenking, J. A. Gladysz, *J. Am. Chem. Soc.* **1997**, *119*, 775–788.
[49] M. I. Bruce, P. Hinterding, P. J. Low, B. W. Skelton, A. H. White, *J. Chem. Soc. Dalton Trans.* **1998**, 467–473.
[50] M. I. Bruce, B. D. Kelly, B. W. Skelton, A. H. White, *J. Organomet. Chem.* **2000**, *604*, 150–156.
[51] M. I. Bruce, P. J. Low, K. Costuas, J. F. Halet, S. P. Best, G. A. Heath, *J. Am. Chem. Soc.* **2000**, *122*, 1949–1962.
[52] M. I. Bruce, P. J. Low, M. Z. Ke, B. D. Kelly, B. W. Skelton, M. E. Smith, A. H. White, N. B. Witton, *Aust. J. Chem.* **2001**, *54*, 453–460.
[53] U. H. F. Bunz, *Angew. Chem.* **1994**, *106*, 1127–1131; *Angew. Chem. Int. Ed. Engl.* **1994**, *33*, 1073–1076.
[54] F. Coat, M. Guillemot, F. Paul, C. Lapinte, *J. Organomet. Chem.* **1999**, *578*, 76–84.
[55] F. Coat, C. Lapinte, *Organometallics* **1996**, *15*, 477–479.
[56] F. Coat, M. A. Guillevic, L. Toupet, F. Paul, C. Lapinte, *Organometallics* **1997**, *16*, 5988–5998.
[57] R. Dembinski, T. Lis, S. Szafert, C. L. Mayne, T. Bartik, J. A. Gladysz, *J. Organomet. Chem.* **1999**, *578*, 229–246.
[58] R. Dembinski, T. Bartik, B. Bartik, M. Jaeger, J. A. Gladysz, *J. Am. Chem. Soc.* **2000**, *122*, 810–822.
[59] S. B. Falloon, S. Szafert, A. M. Arif, J. A. Gladysz, *Chem. Eur. J.* **1998**, *4*, 1033–1042.
[60] F. J. Fernandez, O. Blacque, M. Alfonso, H. Berke, *Chem. Commun.* **2001**, 1266–1267.
[61] G. Frapper, M. Kertesz, *Inorg. Chem.* **1993**, *32*, 732–740.
[62] J. Gil-Rubio, M. Laubender, H. Werner, *Organometallics* **2000**, *19*, 1365–1372.
[63] V. Grosshenny, A. Harriman, R. Ziessel, *Angew. Chem.* **1995**, *107*, 1211–1214; *Angew. Chem. Int. Ed. Engl* **1995**, *34*, 1100–1102.
[64] M. Guillemot, L. Toupet, C. Lapinte, *Organometallics* **1998**, *17*, 1928–1930.
[65] A. Harriman, R. Ziessel, *Chem. Commun.* **1996**, 1707–1716.
[66] M. J. Irwin, G. C. Jia, N. C. Payne, R. J. Puddephatt, *Organometallics* **1996**, *15*, 51–57.
[67] S. Kheradmandan, K. Heinze, H. W. Schmalle, H. Berke, *Angew. Chem.* **1999**, *111*, 2412–2415; *Angew. Chem. Int. Ed.* **1999**, *38*, 2270–2273.
[68] O. Lavastre, J. Plass, P. Bachmann, S. Guesmi, C. Moinet, P. H. Dixneuf, *Organometallics* **1997**, *16*, 184–189.
[69] S. Le Stang, F. Paul, C. Lapinte, *Inorg. Chim. Acta* **1999**, *291*, 403–425.
[70] N. Lenarvor, C. Lapinte, *J. Chem. Soc. Chem. Commun.* **1993**, 357–359.
[71] J. N. Onuchic, D. N. Beratan, *J. Am. Chem. Soc.* **1987**, *109*, 6771–6778.
[72] D. Osella, L. Milone, C. Nervi, M. Ravera, *Eur. J. Inorg. Chem.* **1998**, 1473–1477.
[73] F. Paul, J. Y. Mevellec, C. Lapinte, *J. Chem. Soc. Dalton Trans.* **2002**, 1783–1790.
[74] F. Paul, W. E. Meyer, L. Toupet, H. J. Jiao, J. A. Gladysz, C. Lapinte, *J. Am. Chem. Soc.* **2000**, *122*, 9405–9414.
[75] T. Ren, G. Zou, J. C. Alvarez, *Chem. Commun.* **2000**, 1197–1198.
[76] J. P. Selegue, *Abstr. Pap. Am. Chem. Soc.* **1982**, *184*, 5-Inor.
[77] Y. Sun, N. J. Taylor, A. J. Carty, *Organometallics* **1992**, *11*, 4293–4300.
[78] M. D. Ward, *Chem. Ind.* **1997**, 640–645.
[79] H. Ogawa, T. Joh, S. Takahashi, K. Sonogashira, *J. Chem. Soc. Chem. Commun.* **1985**, 1220–1221.
[80] H. Ogawa, K. Onitsuka, T. Joh, S. Takahashi, Y. Yamamoto, H. Yamazaki, *Organometallics* **1988**, *7*, 2257–2260.
[81] R. M. Bullock, F. R. Lemke, D. J. Szalda, *J. Am. Chem. Soc.* **1990**, *112*, 3244–3245.
[82] F. R. Lemke, D. J. Szalda, R. M. Bullock, *J. Am. Chem. Soc.* **1991**, *113*, 8466–8477.
[83] J. A. Ramsden, W. Q. Weng, A. M. Arif, J. A. Gladysz, *J. Am. Chem. Soc.* **1992**, *114*, 5890–5891.
[84] S. Kheradmandan, Ph.D. Thesis, University of Zürich, **2001**.
[85] E. O. Fischer, H. Leipfinger, *Z. Naturforsch. Teil B* **1955**, *10*, 353–355.
[86] G. Wilkinson, F. A. Cotton, J. M. Birmingham, *J. Inorg. Nucl. Chem.* **1956**, *2*, 95–113.
[87] D. Unseld, Ph.D. Thesis, University of Zürich, **1999**.
[88] C. G. Howard, G. S. Girolami, G. Wilkinson, M. Thornton-Pett, M. B. Hursthouse, *J. Am. Chem. Soc.* **1984**, *106*, 2033–2040.
[89] J. Heck, W. Massa, P. Weinig, *Angew. Chem.* **1984**, *96*, 699–700; *Angew. Chem. Int. Ed. Engl.* **1984**, *23*, 722–723.
[90] S. Kheradmandan, H. W. Schmalle, H. Jacobsen, O. Blacque, T. Fox, H. Berke, M. Gross, S. Decurtins, *Chem. Eur. J.* **2002**, *8*, 2526–2533.
[91] N. Hebendanz, F. H. Kohler, G. Muller, J. Riede, *J. Am. Chem. Soc.* **1986**, *108*, 3281–3289.
[92] a) F. H. Kohler, B. Schlesinger, *Inorg. Chem.* **1992**, *31*, 2853; b) H. Jacobsen, H. Berke, *Chem. Eur. J.* **1997**, *3*, 881–886.
[93] a) D. C. Young, *Computational Chemistry: A Practical Guide for Applying Techniques to Real-World Problems* Wiley, New York **2001**; b) P. Belanzoni, N. Re, A. Sgamellotti, C. Floriani, *J. Chem. Soc. Dalton Trans.* ***1998***, 1825–1835.
[94] a) E. R. Schilling, R. Hoffmann, D. L. Lichtenberger, *J. Am. Chem. Soc.* **1979**, *101*, 585–591; b) D. M. Hoffmann, R. Hoffmann, C. R. Fisel, *J. Am. Chem. Soc.* **1982**, *104*, 3858–3875; c) T. A. Albright, J. K. Burdett, M.-H. Whangbo, *Orbital Interactions in Chemistry*, Wiley, Toronto, Canada, **1985**.
[95] a) A. I. Kulak, A. I. Kokorin, D. Meissner, V. G. Ralchenko, I. I. Vlasov, A. V. Kondratyuk, T. I. Kulak, *Electrochem. Commun.* **2003**, *5*, 301–305; b) J. S. Zhao, A. P. Gu, S. Y. He, R. Choukroun, L. Valade, P. Cassoux, *Acta Chim. Sin.* **2002**, *60*, 687–691; c) F. Cataldo, *Fullerene Sci. Technol.* **2001**, *9*, 525–530.
[96] U. Ruschewitz, P. Muller, W. Kockelmann, *Z. Anorg. Allg. Chem.* **2001**, *627*, 513–522.
[97] F. Cataldo, *J. Macromol. Sci. Pure Appl. Chem.* **2000**, *37*, 881–892.
[98] F. Cataldo, D. Capitani, *Mater. Chem. Phys.* **1999**, *59*, 225–231.
[99] Y. Sun, N. J. Taylor, A. J. Carty, *Organometallics* **1992**, *11*, 4293–4300.
[100] M. Bigorgne, A. Loutelli, M. Pankowsk, *J. Organomet. Chem.* **1970**, *23*, 201–208.
[101] J. G. Verkade, *Coord. Chem. Rev.* **1972**, *9*, 1–106.
[102] N. S. Hush, *Coord. Chem. Rev.* **1985**, *64*, 135–157.
[103] N. S. Hush, *Prog. Inorg. Chem.* **1967**, *8*, 391–444.
[104] M. V. Russo, C. Lo Sterzo, P. Franceschini, G. Biagini, A. Furlani, *J. Organomet. Chem.* **2001**, *619*, 49–61.
[105] T. Weyland, K. Costuas, L. Toupet, J. F. Halet, C. Lapinte, *Organometallics* **2000**, *19*, 4228–4239.
[106] M. Younus, N. J. Long, P. R. Raithby, J. Lewis, *J. Organomet. Chem.* **1998**, *570*, 55–62.
[107] M. B. Robin, P. Day, *Adv. Inorg. Chem. Radiochem.* **1967**, *10*, 247–422.
[108] R. J. Burt, J. Chatt, W. Hussain, G. J. Leigh, *J. Organomet. Chem.* **1979**, *182*, 203–206.
[109] D. N. Hendrick, Y. S. Sohn, H. B. Gray, *Inorg. Chem.* **1971**, *10*, 1550.
[110] L. Brandsma, *Preparative Acetylenic Chemistry*, 2nd ed., Elsevier, Amsterdam, **1988**.
[111] STOE-IPDS Software package Version 2.87 5/1998; STOE & Cie, GmbH, Darmstadt (Germany), **1998**.
[112] G. M. Sheldrick, SHELXL-97, Program for refinement of crystal structures, University of Göttingen (Germany), **1997**.
[113] G. M. Sheldrick, *Acta Crystallogr. Sect. A* **1996**, *46*, 467.

[114] A. L. Spek, PLATON-91, A computer program for the graphical representation of crystallographic models, University of Utrecht (The Netherlands), **1991**.
[115] A. L. Spek, PLUTON, A computer program for the graphical representation of crystalographic models, University of Utrecht (The Netherlands), **1991**–**1997**.
[116] TURBOMOLE, Program package for ab initio electronic structure calculations, Theoretical Chemistry, University of Karlsruhe (Germany), http://www.turbomole.com; a) R. Ahlrichs, M. Bär, M. Häser, H. Horn, C. Kölmel, *Chem. Phys. Lett.* **1989**, *162*, 165–169; b) O. Treutler, R. Ahlrichs, *J. Chem. Phys.* **1995**, *102*, 346–354; c) M. von Arnim, R. Ahlrichs, *J. Comput. Chem.* **1998**, *19*, 1746–1757.
[117] S. H. Vosko, L. Wilk, M. Nusair, *Can. J. Phys.* **1980**, *58*, 1200–1211.
[118] A. D. Becke, *Phys. Rev. A* **1988**, *38*, 3098–3100.
[119] a) J. P. Perdew, *Phys. Rev. B* **1986**, *33*, 8822–8824; b) J. P. Perdew, *Phys. Rev. B* **1986**, *34*, 7406.
[120] a) K. Eichkorn, O. Treutler, H. Öhm, M. Häser, R. Ahlrichs, *Chem. Phys. Lett.* **1995**, *240*, 652–660; b) K. Eichkorn, F. Weigand, O. Treutler, R. Ahlrichs, *Theor. Chem. Acc.* **1997**, *97*, 119–124.
[121] a) A. Schäfer, C. Huber, R. Ahlrichs, *J. Chem. Phys.* **1994**, *100*, 5829–5835; b) A. Schäfer, H. Horn, R. Ahlrichs, *J. Chem. Phys.* **1992**, *97*, 2571–2577.

Received: February 12, 2004
Published online: August 17, 2004

